

1 **Eocene ultra high temperature (UHT) metamorphism in the Gruf complex (Central Alps):**
2 **constraints by LA-ICPMS zircon and monazite dating in petrographic context.**

3 Christian Nicollet^{1*}, Valérie Bosse¹, Maria Iole Spalla² & Federica Schiavi¹

4 ¹*Laboratoire Magmas et Volcans, Université Clermont Auvergne, CNRS, IRD, OPGC, F-63000*
5 *Clermont-Ferrand, France*

6 ²*Dipartimento di Scienze della Terra "A. Desio", Università degli Studi di Milano, Via Mangiagalli*
7 *34, 20133 Milano, Italia.*

8 **Corresponding author (e-mail:Christian.nicollet@uca.fr)*

9 The Gruf complex in the Lepontine Alps is one of the rare occurrences of Phanerozoic UHT
10 metamorphism in the world but its age is still a matter of debate. Here we present LA-ICPMS
11 dating in petrographic context of zircon and monazite from an UHT restitic granulite. Zircons and
12 monazites are both included in large crystals and in retrograde symplectites. In such restitic rocks,
13 partial melting or fluid interactions are unlikely precluding resetting of the monazite chronometers.
14 Zircon cores yield Permian ages interpreted as age of charnockitisation. They are sometimes
15 surrounded by a narrow rim at 32 Ma. Monazites are strongly zoned, but all yield a 31.8 ± 0.3 Ma
16 age interpreted as the time of complete (re-)crystallisation during the UHT paragenesis. We propose
17 that the zircons dated a post Hercynian metamorphism which is responsible of the widespread
18 formation of granulites in the Southern Alps and the crust differentiation. This fluid-absent melting
19 event produced refractory lithologies such as restites in charnockites. We suggest that Gruf UHT
20 paragenesis is alpine in age and crystallised from these refractory lithologies. We conclude that the
21 lower restitic crust produced at the Permian time had the ability to achieve UHT conditions during
22 the fast exhumation and heating related to lithospheric thinning in Alpine time.

23 **Supplementary material:** Analytical procedures for monazite analysis and dating; table of major
24 elements of the minerals; table of the isotope data; table of trace element measurements in zircon

25 **Introduction**

26 The Gruf complex in the Lepontine Alps is one of the rare occurrences of Phanerozoic UHT
27 metamorphism in the world, discovered in the Val Codera by Cornelius (1916), Cornelius & Dittler
28 (1929), and described by Barker (1964), Wenk et al. (1974). Because occurrences of UHT
29 metamorphism are mainly of Precambrian age (eg Harley, 1998; Brown, 2007; Kelsey and Hand,
30 2015), this area is of major interest to understand the geodynamic signification of such extreme
31 metamorphic conditions. Indeed, the main difficulty in understanding the geodynamic significance
32 of UHT metamorphism is that Precambrian UHT granulites are often preserved in small-scale

33 lenses: they usually represent structural and metamorphic relics in polymetamorphic rocks
34 belonging to polycyclic terrains. The lack of large-scale tectonic structures associated to their
35 emplacement precludes a clear understanding of their geodynamic history. Thereby the few
36 Phanerozoic UHT occurrences for which the geological context is well constrained are precious
37 records that help to understand and interpret this type of metamorphism.

38 The age of the UHT metamorphism in the Gruf complex is currently a matter of debate. Based on
39 zircon U/Pb dating, Galli et al. (2012) have proposed a Permian age (282 – 260 Ma) for the
40 granulite facies fluid-absent biotite melting event. For these authors, the presence of orthopyroxene
41 inclusions in zircons confirms the Permian age of the charnockites and associated sapphirine-
42 bearing granulites. Zircon rims from the same samples yield 34-29 Ma ages interpreted as dating
43 the Alpine amphibolite facies migmatization. A different interpretation was suggested by Droop and
44 Bucher (1984) and proposed by Liati and Gebauer (2003). The latter authors considered that the
45 zircon Alpine rims (yielding a weighted mean age at 32.7 ± 0.5 Ma in their samples) grew during
46 the UHT metamorphic event, and that the sapphirine-bearing granulites were restites formed during
47 partial melting of the Permian granitoids. Moreover, Schmitz et al. (2009) measuring an age of 33.0
48 ± 4.4 by monazite chemical dating also agree with this interpretation.

49 These contrasting results imply two different models for the origin of the ultra-high temperature
50 (UHT) metamorphism: 1) a Permian UHT metamorphism can be linked to the post Hercynian high-
51 thermal regime, associated with lithospheric Permian-Triassic thinning and responsible for the
52 widespread formation of granulites in the Austroalpine and South -Alpine continental crust (e.g.:
53 Brodie et al., 1989; Lardeaux and Spalla, 1991; Diella et al., 1992; Barboza and Bergantz, 2000;
54 Muntener et al. 2000; Schuster et al., 2001; Spalla and Marotta, 2007; Schuster and Stuewe 2008;
55 Galli et al., 2013; Spalla et al., 2014). This anomalously high thermal regime would be responsible
56 for a pervasive melting event, associated with melt loss leading to the genesis of a residual,
57 refractory lower crust. Such processes are interpreted to be responsible of the lower continental
58 crust differentiation (e.g. Vielzeuf and Holloway, 1988; Brown, 2008; Redler et al., 2013); 2) An
59 Alpine UHT metamorphism would have been driven by lithospheric thinning associated with slab
60 breakoff and asthenospheric upwelling ((e.g. Davies and von Blanckenburg, 1995; von
61 Blanckenburg and Davies, 1995; Oalman et al., 2016) which would provide the considerable
62 amount of heat necessary to reach the UHT conditions.

63 In this study, we combine for the first time zircon and monazite in situ dating in petrographic
64 context for the Gruf sapphirine bearing granulite. The results provide a new opportunity to clarify
65 the age of the UHT event and its geodynamic context.

66

67 **Geological setting**

68 Penninic nappes in the Central Alps consist of variegated rocks of continental and oceanic origins.
69 This nappe stack is separated from the Southern Alps by the Periadriatic Lineament and by a thin
70 ribbon of Austroalpine crust verticalised along the “southern steep belt” (e.g. Schmid et al., 1996).
71 The axial portion of Central Alps has recorded a polycyclic metamorphic evolution: structural and
72 petrologic relics of Hercynian and Caledonian imprints have been described (Schaltegger, 1994;
73 Spalla et al., 2014 and refs therein). The Alpine overprint occurs with heterogeneous intensity, and
74 the separation of Alpine from pre-Alpine metamorphic imprints has remained for a long time
75 difficult due to the similar metamorphic conditions associated with these successive orogenic cycles
76 (e.g.: Niggli, 1974; Engi et al., 2004). Alpine metamorphism in the Central Alps is characterized by
77 a polyphasic metamorphic evolution characterised by an early high pressure- low- to intermediate-
78 temperature imprint, preserved as relic blueschist- and eclogite-facies assemblages, recorded during
79 the south-verging subduction. The second metamorphic imprint is characterised by assemblages
80 indicating a Barrow-type event interpreted as consequent to the continental collision. Isograds of the
81 Barrovian metamorphism define the “Lepontine metamorphic dome” (Trommsdorff, 1966; Todd
82 and Engi, 1997) and their concentric distribution indicates that metamorphic conditions increase
83 southwards from greenschists- to upper amphibolite-facies. In this southern part partial melting
84 conditions have been attained at about 700°C and 0.6-0.8 GPa between 32 and 22 Ma (Engi et al.,
85 1995; Burri et al, 2005; Berger et al, 2009; Rubatto et al., 2009). The Gruf complex (Fig. 1) is a
86 small tectonic unit of about 200 km², located in the southeastern part of the Lepontine dome, north
87 of the Insubric Line, and limited to the east by the calc-alkaline Tertiary intrusive stock of Bergell.
88 This intrusive massif is considered synchronous with crustal anatexis at 33 - 28 Ma (Berger et al.
89 1996). The Gruf complex is composed mainly of biotite-garnet-sillimanite-cordierite metapelitic
90 rocks and migmatitic orthogneisses and paragneisses, and has been recently considered as part of
91 the tectonic mélange of continental and oceanic units accreted together in the Alpine tectonic
92 accretion channel (Engi et al., 2001). During a remarkable field work in a very difficult terrain Galli
93 et al. (2012) described structural and petrologic characters of the complex in situ for the first time,
94 focusing especially the Mg-Al-rich sapphirine granulites. The latter form schlieren and residual
95 enclaves within sheet like bodies of charnockites and migmatitic orthogneisses (Galli et al., 2013).
96 The chemical composition of the Mg-Al-rich granulites is comparable to that of restitic
97 surmicaceous enclaves in granites (e.g. Montel et al., 1991) except for magnesium. Kelsey et al.
98 (2003) suggested that the production of Mg-Al-rich compositions through melt loss is improbable
99 because of the low Mg partition into melt. For these authors Mg-rich assemblages may source from
100 Mg-enriched protoliths. Consequently, the Gruf Mg-Al-rich sapphirine granulites may represent
101 resister lenses within charnockites/orthogneisses or restites from Mg-rich protolith included in the

102 charnockites.

103 Previous published geochronological studies are at the origin of the contrasted interpretations for
104 the geodynamic signification of the UHT conditions recorded in the Gruf complex. Liati and
105 Gebauer (2003) report SHRIMP weighted mean ages at 272.0 ± 4.1 Ma in zircon cores and at 32.7
106 ± 0.5 Ma in zircon rims from a sapphirine bearing granulite sample. The Permian ages are
107 interpreted as reflecting the age of the magmatic protolith whereas the Alpine ages are considered to
108 represent the age of the granulite facies metamorphism. For these authors, sapphirine-bearing
109 granulites represent restites formed during Alpine partial melting of Permian granitoids. Galli et al.
110 (2011; 2012) proposed different interpretation based on similar geochronological data obtained with
111 the same method (Zircon SHRIMP analyses). For these authors 282-260 Ma ages obtained in
112 oscillatory zoned zircon cores represent melts generated through granulite facies fluid-absent biotite
113 melting at 920-940°C in metapelitic rocks, whereas 34-29 Ma ages in zircon rims date the Alpine
114 amphibolite facies migmatization. For these authors the charnockites associated with the sapphirine-
115 bearing granulites belong to the post-Hercynian European lower crust. Schmitz et al. (2009) applied
116 the method of 3D-Micro X-ray fluorescence analysis on monazite in thin section from a sapphirine-
117 bearing granulite. They obtained an age at 33.0 ± 4.4 Ma in monazites included in and intergrown
118 with HT minerals which they interpreted as the age of the high-temperature event. Finally, Oalman
119 et al. (2013, 2016) also suggest that UHT conditions were reached slightly before 32.5 Ma followed
120 by cooling from 30 to 19 Ma recorded by rutile $^{206}\text{Pb}/^{238}\text{U}$ ages.

121

122 **Petrography of the Mg-Al granulites**

123 Mg-Al-rich sapphirine granulites have been already carefully described by Barker (1964), Droop
124 and Bucher (1984), Galli et al., (2011) and Guevara and Caddick (2016). We will concentrate here
125 on the main petrological characters and mineral reactions, which appear to be of major interest to
126 link petrology and geochronology. The studied sample is a pebble which has been collected in upper
127 Val Codera (Fig. 1). Two domains have been recognized at the sample scale: one is a sapphirine-
128 bearing granulite (Fig. 2a; 3/4 of the sample)) while the other has the typical mineralogy of a
129 charnockite (Figs. 2d and e; 1/4 of the sample). The boundary between these two domains is
130 progressive. Composition of the granulitic domain is enigmatic. Galli et al. (2011) propose that the
131 granulitic domain could be a restite/schlieren of Mg-rich métapélite. It could be a restite of an
132 unknown (magnesian ?) protolith within the charnockitic domain. The charnockitic paragenesis is
133 composed of millimetric to pluri-millimetric crystals of Opx - Bt - Kfs \pm Pl - Qz - Mnz - Zrn and Ap
134 (Figs. 2d and e; abbreviations in text and figures are from Whitney and Evans (2010)). Rare
135 inclusions of zircon, monazite, plagioclase and quartz are observed in the phenocrysts. In some

136 places, clusters of K-feldspar - quartz-apatite microcrysts are following the grain boundaries in the
137 charnockitic assemblage (Fig. 2e). They seem to represent incipient melting or residual melt after
138 extraction. In the charnockite domain, K-feldspar is orthose (XOr: 80%; XAb: 20%), plagioclase
139 has an intermediate composition with XAn: 40. The compositions of orthopyroxene and biotite are
140 substantially the same as in the granulitic domain of the rock.

141 The primary crystals of the residual/resister granulite are millimetric to plurimillimetric. The peak
142 UHT paragenesis was: Al rich-Opx - Sil - Spr - Bt - Grt - Crd - Rt - Ap - Zrn - Mnz (Fig. 2a). Here
143 again some tiny inclusions are rarely present. Detailed observations of the mineral associations
144 reveal complex relationships with (at least) 2 generations of Al-rich orthopyroxene, sillimanite,
145 cordierite and sapphirine ± spinel ± biotite, garnet and rare inclusions of quartz, rutile and apatite.
146 Secondary minerals are abundant. Except for orthopyroxene, the chemical composition of the
147 minerals does not change much and the crystals are weakly zoned (Table A supplementary
148 material). Garnet is almost pure almandine – pyrope solid solution with a slight decrease of pyrope
149 relative to almandine at the rim of the crystals (from the core to the rim: XPy: 48-46 %; XAlm: 42-
150 45 %). Grossular and spessartine contents are low: XGr: 2.2-3.1% and XSp: ≤1%. Opx is Al₂O₃-
151 rich and zoned (core: 7.5-8.6% and rim: 5.5 to 7 % Fig. 3). Biotite is Mg- (XMg: 75-80%) and Ti-
152 rich (TiO₂: 2.6-3.6%). Cordierite composition is homogeneous both in primary minerals and in
153 symplectites. Galli et al. (2011), Oalmann et al. (2013), Guevara and Caddick (2016) estimated the
154 conditions of the primary paragenesis in these granulites at T = 920-940 °C and P= 0.85-0.95 GPa.

155 The secondary symplectites in the granulites are varied and complex, with Spr, Sil, Crd, Opx ± Sp.
156 Spinel is hercynite - spinel solution, homogeneous in composition. Two main reactions dominate
157 (Fig. 2b-c): Sil 1 phenocrysts are surrounded by Spr 2 + Crd 2 in contact with Opx ± Bt; the garnet
158 is destabilized into symplectites of Opx 2 + Crd 2. These two reactions indicate a pressure decrease.
159 Al₂O₃ content in Opx 2 is between 7.4 to 5.9 % similar to the rims of the primary phenocrysts (Fig.
160 3) whereas the XMg is slightly lower than in the primary crystals. Primary Opx probably continues
161 to grow at the beginning of the retrograde evolution during decompression, while garnet is
162 destabilized. This suggests that primary paragenesis and retrograde symplectites are the product of a
163 single metamorphic event. These retrograde textures demonstrate a re-equilibration of the UHT
164 peak assemblages at lower metamorphic conditions: 720-740 °C at 6.5-7.5 kbar which starts with a
165 decompression and continue with a temperature decrease (Galli et al. 2011; Oalmann et al. 2013;
166 Guevara and Caddick, 2016). These conditions are similar to those inferred for the migmatization
167 occurring during the Tertiary Barrovian regional metamorphism (Burri et al, 2005; Engi et al.,
168 1995).

169 Both zircons and monazites are included in the large crystals (namely primary phenocrysts) :

170 orthopyroxene, orthoclase from the charnockitic assemblage ; sapphirine, orthopyroxene,
171 sillimanite, cordierite from the UHT assemblage as well as in the cordierite – biotite matrix and in
172 the late symplectites. Mineral inclusions are rare in garnet and zircon and monazite have not been
173 detected in it.

174 **Zircon and monazites textures**

175 Zircons are subhedral elongated and/or resorbed rounded crystals 30-100 μm long. They contain
176 rare and very tiny inclusions among which biotite, white mica, quartz and apatite were only
177 unequivocally identified by Raman spectrometry. Sillimanite has not been observed. Zircons
178 included in the primary phenocrysts of the two domains are resorbed grains and seem to be relictual
179 (Fig. 4a). Cathodoluminescence images (CLI) show that most of the grains display a large inner
180 domain with usually oscillatory or rarely complex zoning (Fig. 4b - c). In zircon included in
181 cordierite – biotite matrix and in late symplectites, this inner domain is sometimes surrounded by a
182 thin rim ($<5 \mu\text{m}$ to $15 \mu\text{m}$) with euhedral faces and bright in CDI (Fig. 4c). U and Th contents are
183 variable ($150 < \text{U} < \sim 4860$ ppm and $4 < \text{Th} < 1180$ ppm; Table B supplementary material) with no
184 correlation with the internal structure nor ages (see the next section). As a result, Th/U ratios are
185 also variable ($0 < \text{Th}/\text{U} < 0.50$) and not related to the different zircon domains (i.e. oscillatory zoned
186 inner domain or external rim). Trace elements have been analysed in the core and in the rims of the
187 zircon grains. Because the rims are very thin compared to the spot size ($15 \mu\text{m}$), we were not able to
188 analyse properly the rims. Rare earth elements (REE) pattern of the zircons show an enriched
189 distribution of the heavy REE, negative Eu anomalies ($\text{Eu}/\text{Eu}^* = 0.05 - 0.09$) and positive Ce
190 anomalies (see Supplementary material – Table C) which are similar to those described in zircon
191 from Grt-bearing granulite facies rocks (Rubatto et al. 2002). Zircons from the charnockite domain
192 display same REE pattern as those of granulite.

193 Monazites are 50 to 150 μm in size and are present in the core of large Spr, Opx, Crd crystals or
194 form clusters of small grains (10 to 40 μm) in the late symplectites. The shape of the grains varies
195 from large rounded grains to small elongated ones with rarely indented grain boundaries (Fig 5b
196 and 6a), without any correlation with the textural position. Rare inclusions are needles of sillimanite
197 (Fig. 6a). All the grains are strongly zoned (Table 1). Chemical variations of the LREE-, Th- and
198 Ca-contents broadly follow the brabantite substitution ($2\text{REE}^{3+} = \text{Th}^{4+} + \text{Ca}^{2+}$). ThO₂ content varies
199 from 1.3 to 10.8 wt%. Y₂O₃ and UO₂ contents are highly variable (from 0.1 to 5.5 wt% and from
200 0.2 to 3.5 wt%, respectively) and inversely correlated. These variations are clearly related to
201 mineral position within the sample (Fig. 7a): monazites in the charnockite domain are Y-rich and U-
202 poor whereas the opposite is true in the granulite domain. Variations in LREE, MREE and Y₂O₃
203 contents are also correlated to the sample zonation: monazites from the charnockite domain are

204 enriched in Gd_2O_3 and Y_2O_3 whereas monazites from the granulite domain are enriched in La_2O_3
205 and poor in Gd_2O_3 and Y_2O_3 (Fig. 7 b - c). Chemical variations are observed from grain to another
206 but also within single crystal: for example T50M1 crystal on Fig. 6 a and 7 in the Al-granulite
207 domain; T14M1 crystal on Fig. 7 and T12M1 crystal on Fig. 6 b in the charnockite domain. Some
208 of the grains display very tiny Y-rich overgrowths (Fig. 6a).

209 **U-Th-Pb geochronology**

210 Monazite and zircon have been analysed in thin section by LA-ICPMS in order to control the
211 position of the grain (and thus the measured ages) relative to the textures observed in the sample.
212 Zircons and monazites were ablated using a Resonetics Resolution M-50 equipped with a 193 nm
213 Excimer laser system coupled to an Agilent 7500 cs ICP-MS with a 1 Hz repetition rate, a fluence
214 of 7 J/cm² and a spot size of 7 μ m for monazite dating and 3 Hz repetition rate, a fluence of 2.6
215 J/cm² and a spot size of 20 μ m for zircon dating. Helium carrier gas was supplemented with N₂
216 prior to mixing with Ar for sensitivity enhancement (Paquette et al., 2014). Detailed analytical
217 procedures are reported in Paquette and Tiepolo (2007) and Didier et al. (2015) and in
218 Supplementary – Analytical procedures. Monazite can be dated using both U-Pb and Th-Pb decay
219 schemes. Here we will only consider $^{208}Pb/^{232}Th$ ages for the following reasons. Firstly, ^{232}Th is
220 largely predominant in monazite, allowing small spots (7 μ m) to be performed during laser ablation.
221 Secondly, U decay series could be in disequilibrium in young monazites (Schärer, 1984), resulting
222 in overestimated $^{206}Pb/^{238}U$ ages. Because secular equilibrium among the intermediate daughters of
223 ^{232}Th occurs after about 30 years, it seems reasonable to assume that initial ^{208}Pb is absent. Thirdly,
224 ^{232}Th is so abundant that ^{208}Pb originating from common Pb is usually negligible compared to
225 radiogenic ^{208}Pb . To reinforce this hypothesis, we only consider here the concordant $^{208}Pb/^{232}Th$ –
226 $^{206}Pb/^{238}U$ ages (Fig. 8a). Whatever the textural position of the monazite grains or the chemical
227 composition of the monazite domain, the $^{208}Pb/^{232}Th$ ages are between 29.6 ± 1.0 and 34.1 ± 1.1
228 Ma, allowing to calculate a weighted average age of 31.8 ± 0.3 Ma (MSWD = 3,2, N = 51; Fig. 8b;
229 Supplementary material: Table B). We notice the important chemical variations in the same crystal,
230 but identical ages (Figs. 6 and 7). This suggests significant chemical transfer and/or variation of the
231 redox state through the rock during this brief metamorphic episode of UHT.

232 $^{206}Pb/^{238}U$ ages measured in zircon from our sample are scattered from 30 ± 1 to 304 ± 12 Ma (only
233 U/Pb concordant ages; Fig. 8c). Ages are similar in the charnockite and granulite domains. The
234 youngest ages have been obtained in the bright rims. Plotted in a Tera Wasserburg diagram, we see
235 that these ages are in total agreement with the ages measured in the monazite grains (Fig. 8c). The
236 oldest ages are upper Carboniferous-lower Permian and have been obtained in the inner oscillatory
237 zoned domains. Two reasons can be provided to explain intermediate ages between the oldest and

238 the youngest ones: i) they reflect mixing between the Carboniferous core and the narrow Cenozoic
239 rim (<5 μm to 15 μm) due to analysis of distinct adjacent domains; ii) they result from Pb loss.
240 Indeed, in some of the grains the U content is high (U > 1000 ppm). Such a high U content could be
241 responsible for radiation damage of the crystal lattice especially in Paleozoic zircons and induce Pb
242 loss. This results in younger core compared to the rim as observed in Figure 4b. With the aim of
243 limiting these two effects and to better restrict the range of the oldest ages, we decide to only
244 consider the ages which were measured i) in the zircon crystals which do not present the
245 luminescent rim on the CLI, ii) measured in domains with U content ≤ 1000 ppm. By doing this the
246 scattering of the $^{206}\text{Pb}/^{238}\text{U}$ ages remains between 247 ± 6 and 304 ± 12 Ma (Fig. 8d).

247

248 **Discussion**

249 **▪ Ages recorded in zircon**

250 Two groups of ages have been recorded in the zircons: between 247 ± 6 and 304 ± 12 Ma in the
251 core and ca 30 Ma in the rim. These ages are in total agreement with the results obtained by Liati
252 and Gebauer (2003) and Galli et al. (2012). Following these last authors, who found the
253 charnockitic paragenesis included within the zircon cores, the ages measured in the oscillatory
254 zoned inner domain could be interpreted as the age of the charnockitisation. As no older inherited
255 domains have been observed in our zircons, we favour this interpretation. This charnockitisation
256 can be developed under the Permian-Triassic high-thermal regime (Galli et al., 2013) responsible of
257 the widespread formation of granulites in the Southern Alps and Austroalpine (Bertotti et al., 1993;
258 Spalla and Marotta, 2007; Spalla et al., 2014 and references herein). The scattering of the ages
259 between 247 to 304 Ma in a single sample is rather surprising and, as previously suggested, can not
260 be only attributed to mixing ages. Such a large spread of zircon ages is known in other Austroalpine
261 and Southalpine units (Marotta et al., 2016 and refs therein) representing lower continental crust:
262 Ivrea zone (Vavra and Schaltegger, 1999; Peressini et al., 2007), Malenco (Müntener et al., 2000),
263 Sondalo (Tribuzio et al., 1999), Valtournanche (Manzotti et al, 2012). Vavra and Schaltegger (1999)
264 suggest that the U-Pb system in zircons from the Ivrea Zone could have been disturbed by different
265 types of alteration and Pb-loss processes during the Permian, Triassic and possibly early Jurassic
266 times. These perturbations were differently interpreted as consequent to the early stages of
267 Mesozoic rifting related to thermal and/or decompression pulses during extensional unroofing in the
268 Permian (Marotta et al., 2009), as for example in Valtournanche, where the pre-Alpine evolution is
269 associated with LP-HT metamorphism related to Permian-Triassic lithospheric thinning (Manzotti
270 et al, 2012; Manzotti & Zucali, 2013). Our results, although slightly older than the previously
271 published ages (but within 2σ error bar), are in agreement with these interpretations.

272 The second group of ages between 30 ± 1 Ma and 34 ± 2 Ma has been recorded in euhedral rims
273 from some crystals included in the Bt-Crd matrix or Spr-Crd symplectites. Most of the zircons
274 included in the primary phenocrysts do not present such a younger rim (Fig 4 b). Furthermore, these
275 results are similar to the $^{208}\text{Pb}/^{232}\text{Th}$ ages measured in the adjacent monazites, whatever the textural
276 position of the latter. Thus, these results argue for a zircon recrystallisation event at ca. 32 Ma
277 simultaneous with the crystallisation (or re-crystallisation, see the discussion below) of the
278 monazite grains.

279 ▪ Monazite ages

280 Contrary to the zircon results, monazites from the studied sample provide narrow age estimation at
281 31.8 ± 0.3 Ma (between 29.6 ± 1.0 and 34.1 ± 1.1 Ma). The ages are the same in all the different
282 textural positions of the monazite (included in large Spr, Opx or Crd crystals or in the Crd-Bt matrix
283 or as cluster of small grains within secondary symplectites), or the chemical zoning of the granulitic
284 (Fig. 6a) or charnockitic (Fig. 6b) paragenesis. The Y-rich overgrowths observed in some monazite
285 grains which could be related to the garnet destabilisation (Didier et al. 2014) do not yield younger
286 ages (Fig. 6a). Similarly, no older ages (i.e. Paleozoic) have been recorded by the monazites.
287 Usually the shape of the monazite grains suggests equilibrium with, on one hand, the large primary
288 crystals recording the peak of the UHT conditions and on the other hand, with the secondary
289 symplectites during the beginning of the retrograde evolution. This demonstrates that the Spr-Opx-
290 Sil UHT paragenesis as well as the retrograde symplectites in the restitic granulites equilibrated at
291 ca. 32 Ma, in agreement with earlier works (Liati and Gebauer, 2003, Schmitz et al., 2009, Droop
292 and Bucher, 1984). The Alpine UHT event is recorded by the monazite and by the zircon rims.

293 ▪ Age of UHT metamorphism in the Gruf complex

294 Our zircon and monazite age results point to an age of 32 Ma for UHT. Galli et al. (2011, 2012,
295 2013) disagree with this interpretation. In their model, the Alpine age recorded in the zircon rims
296 represents the age of the migmatization of the Gruf lithologies in the upper amphibolite facies
297 conditions. Moreover, they interpreted that the ages recorded at 33.0 ± 4.4 Ma by monazite
298 (Schmitz et al., 2009) are supposedly the result of the monazite resetting during fluid-assisted
299 migmatization (Galli et al. 2012). We cannot support this interpretation for two reasons. First, many
300 examples exist in the literature that show that monazite is a robust geochronometer able to retain
301 age records during anatectic processes (Paquette et al. 2004; Rubatto et al. 2006; Stepanov et al.
302 2012; Rubatto et al. 2013; Didier et al. 2014; Didier et al. 2015) or even UHT conditions
303 (Korhonen et al. 2013; Rocha et al. 2017). The main causes of possible disturbance of the Th-U-Pb
304 systems in monazite are dissolution/recrystallisation processes during melt or hydrous fluid
305 interaction (eg: Cherniak et al., 2004; Kelsey et al. 2012). Fluid interaction in the present context is

306 difficult to argue and in any case supposes an external input (see the next point below).
307 Dissolution/recrystallisation processes during melt interaction strongly depend upon the melt
308 composition and its H₂O content (Montel, 1986; Rapp and Watson 1986; Spear and Pyle 2002).
309 Monazite solubility is low in meta- or peraluminous melts and thus monazite is able to resist to
310 crustal anatexis. To conclude, if fluid-assisted migmatization in the amphibolite conditions occurred
311 during the Alpine times following a Permian UHT event, we would expect to measure Permian ages
312 in part of the monazite domains or grains, which is not the case. “Resetting” cannot be an
313 explanation for the absence of Permian age records in monazite in the present conditions.

314 The second point questions the migmatization processes in such refractory lithologies. As reported
315 by Galli et al. (2011), Mg-Al granulites occur as restites or schlieren in the charnockites and thus
316 represent highly refractory rocks formed during partial melting processes in the Permian times.
317 Partial melting of such refractory lithologies is improbable as also suggested by McDade and
318 Harley (2001) unless a high amount of fluid is added. It is very unlikely that this fluid-assisted
319 migmatization event in the amphibolite facies conditions could be responsible for all the textures
320 observed in the UHT granulites. There is no evidence in the retrograde reactions of significant
321 fluid input as argued by Galli et al. (2011). In contrast we propose that all the metamorphic textures
322 in the Mg-Al granulites correspond to the UHT conditions during the Alpine time, as demonstrated
323 by the age recorded in the monazites equilibrated with the UHT mineral assemblages.

324 ▪ A model for the evolution of the Gruf granulites and charnockites

325 Based on the petrological observations and geochronological results obtained in our sample we
326 propose the following model for the time evolution of the Gruf granulites and charnockites. The
327 oldest ages we obtained in the zircons from our UHT granulite sample are between 304 ± 12 Ma
328 and 247 ± 6 Ma. These ages, despite slightly older, are similar to those measured by Galli et al.
329 (2012) and Liati and Gebauer (2003) in the Gruf UHT granulites. Older ages at 513 ± 8 Ma and 453
330 ± 8 Ma (weighted average ages in magmatic zircon cores) have only been reported in an enclave-
331 rich biotite orthogneiss in the Gruf complex (Galli et al. 2012). Our results suggest that oscillatory
332 zoned zircons from the UHT granulites crystallized in the Permian-Triassic times during a partial
333 melting event. This Paleozoic anatectic event occurred under the granulite facies conditions, as
334 shown by the presence of the charnockitic paragenesis included in the zircon cores (Galli et
335 al. 2013), inducing the formation of both charnockitic melt and restitic/resister rocks, the precursor
336 of the sapphirine-bearing granulites. Unfortunately, the few tiny inclusions observed in the zircon
337 grains do not allow to precise what was the mineral assemblage in this precursor during the
338 Paleozoic event. We suggest that the precursor of the sapphirine-bearing granulites was a biotite –
339 cordierite rich selvage probably containing also orthopyroxene and garnet could have been added.

340 Considering the abundance of the monazites in our sample, it is likely that monazites were present
341 during the Permian times. During the Alpine times, UHT metamorphism occurred during a short-
342 lived event (less than 5 Ma) between 30 to 34 Ma recorded by both zircon rims and monazites.
343 UHT metamorphic conditions at 920-940 °C/ 0.85-0.95 GPa (Galli et al., 2011) are responsible for
344 the complete re-crystallization of both the charnockites and the Bt-Cd-Gr(??)-Opx(??)-bearing rocks
345 and enable the development of UHT parageneses appearance: Al rich-Opx - Sil - Spr - Bt - Grt –
346 Crd – Rt – Ap- Zrn - Mnz in the Mg-Al granulite and Opx, Bt, Kfs, ± Pl, Qz, Zrn, Mnz and Ap in
347 the charnockite. In both the charnockites and the Mg-Al granulites, this UHT event is responsible
348 for the partial dissolution of the Paleozoic zircons and the growth of the Alpine rims. Because no
349 Paleozoic ages were found in monazites from our samples (as well as in the previous monazite
350 study, Schmitz et al. 2009), crystallisation processes for the Alpine monazites are more difficult to
351 assess. Two processes can be proposed: crystallisation from a mineral precursor such as allanite or
352 apatite, or complete recrystallisation of an earlier monazite generation, possibly late Carboniferous
353 – Permian in age. In our sample petrographic evidences of a monazite precursor are missing and it
354 is not possible to solve the question in the present context.

355 ▪ Geodynamic implications and the origin of the UHT metamorphism in the
356 central Alps

357 The oldest ages we obtained in the zircon cores between 304 ± 12 Ma and 247 ± 6 Ma interpreted as
358 the age of the charnockitisation, unknown elsewhere in the Penninic domain of the Central Alps
359 (Galli et al, 2011),), developed during Permian-Triassic high thermal regime responsible for HT-LP
360 metamorphism widespread in the Austroalpine and Southalpine domains (Galli et al., 2013, Barboza
361 and Bergantz, 2000; Lardeaux and Spalla, 1991; Diella et al., 1992; Bertotti et al., 1993; Muntener
362 et al. 2000; Marotta et al., 2016). These granulites are interpreted as residual and refractory rocks
363 following partial melting events and extensive melt loss. This process is responsible for the
364 differentiation of the continental crust via fluid-absent melting reactions involving muscovite and
365 biotite (and amphibole in metabasic rocks) destabilisation. As a consequence, the precursor of the
366 Al-Mg granulites of the Gruf complex acquired its restitic character during this post Hercynian
367 event.

368 UHT metamorphism occurs at temperatures above the fluid-absent melting in most crustal rocks
369 which is an endothermic process that consumes heat and buffers the temperature (Vielzeuf and
370 Holloway, 1988; Stüwe 1995). Thus partial melting limits heat production avoiding a fertile crust to
371 attain UHT. Nevertheless, UHT conditions are more easily reached in refractory/restitic rocks and
372 develop preferentially in terrains that previously underwent metamorphism and melt loss (Clark et
373 al., 2011; Kelsey and Hand, 2015). The Gruf complex is the sole unit in Penninic Domain of Central

374 Alps recording the Permian-Triassic granulitic metamorphism, which permitted its rocks to reach
375 and record UHT conditions during the Alpine cycle.

376 Zircon and monazite ages, together with their microstructural relationships with granulite facies
377 minerals, show that the typical UHT paragenesis crystallised at Alpine time during a short-lived
378 event (less than 5 Ma) between 34 to 30 Ma. These results are in agreement with the garnet
379 diffusion modelling proposed by Galli et al. (2011) also suggesting that UHT metamorphism was
380 brief. This UHT metamorphism is contemporaneous with the Bergell tonalite-granodiorite intrusion
381 dated between 33 and 28 Ma (Berger et al. 1996) and the beginning of the anatectic event in the
382 Southern part of the Central Alps at 32 Ma (Köppel et al, 1981; Berger et al, 2009; Rubatto et al.,
383 2009). Secondary symplectites in the Mg-Al granulites just following the UHT peak conditions are
384 equilibrated in the same conditions as the Lepontine migmatization (e.g. Engi et al. 1995; Burri et
385 al. 2005). However, the 38-34 Ma UHP metamorphism in the Lepontine domain, is quickly
386 followed by a fast exhumation, then the UHT event and the final amphibolite facies migmatization
387 (Brouwer et al. 2004). This fast exhumation is related to a short-lived (less than 4 Ma) episode of
388 lithospheric thinning associated with a rise of hot asthenospheric material (Brouwer et al., 2004)
389 from 34 Ma to 32–30 Ma (Beltrando et al., 2010). Oalman et al. (2016) proposed that similar
390 lithospheric thinning associated with slab breakoff or roll back and asthenospheric upwelling could
391 also be responsible for the short-lived Alpine UHT metamorphism in the Gruf complex. A similar
392 geodynamic context is proposed for another example of Phanerozoic UHT metamorphism (16Ma)
393 of the island of Seram (Indonesia) where the UHT conditions were produced by slab rollback–
394 driven lithospheric extension and the exhumation of hot subcontinental lithospheric mantle
395 (Pownall et al, 2014; Pownall, 2015). Harley (2016) proposed that shorter duration UHT granulite
396 event can be formed as a consequence of severe lithospheric thinning and crustal extension
397 accompanied by voluminous magmatism in arc settings affected by subduction roll-back. Brouwer
398 et al. (2004) notice that heating by slab detachment is fast and transient (more than 100°C in up to
399 10 million years.), whereas radiogenic heating requires time spans of the order of tens of millions of
400 years and cessation of the subduction process. Finally, Perchuk et al. (2017) used numerical models
401 to explain ultra-hot orogeny and showed that UHT conditions at the bottom of the crust might be
402 produced by lateral propagation of the hot asthenospheric front during plate convergence associated
403 with lithospheric delamination. In this model, a close relationship of HT-UHT metamorphism with
404 tonalitic magmatism is proposed which could explain the relation between the Gruf UHT
405 metamorphism and the Bergell intrusion, which is one of the main Periadriatic igneous bodies
406 emplaced during Late Alpine times, characterised by an enriched mantle source (von Blanckenburg
407 et al., 1998), and interpreted as triggered by post-collisional slab break off.

408 **Conclusions**

409 In situ and in context zircon dating on zircon from a restitic granulite within charnockites gives both
410 Permian-Triassic (304- 247 Ma) and Alpine ages (ca 34-30 Ma). $^{208}\text{Pb}/^{232}\text{Th}$ ages measured in
411 monazite from the same sample yield a weighted average age of 31.8 ± 0.3 Ma (MSWD = 3.2; N =
412 51) interpreted as the time of complete (re-)crystallisation of the monazite in equilibrium with the
413 UHT paragenesis. The Alpine UHT event was thus recorded by zircon rims and monazites. The
414 oldest ages we obtained in the zircons between 304 ± 12 Ma and 247 ± 6 Ma are interpreted as the
415 age of the charnockitisation during which the precursor of the Al-Mg granulites of the Gruf
416 complex acquired its restitic character. Our results show that the Gruf complex is the sole Penninic
417 unit in the Central Alps recording the post Hercynian granulitic metamorphism which permits to
418 reach and record UHT conditions during the Alpine cycle. The typical UHT paragenesis crystallised
419 at Alpine time during a short-lived event (less than 5 Ma) related to lithospheric thinning associated
420 with a rise of hot asthenospheric material.

421 **Acknowledgments**

422 The subject editor Igor Villa and the two reviewers Simon Harley and Jean-Marc Lardeaux are
423 thanked for their constructive comments. We also thank Dr. E. Bruand for reading the English.
424 Thanks are due to Jean Luc Devidal and Jean-Marc Hénot for their help in the use of EMP and
425 SEM.

426 **References**

- 427 Barker, F., 1964. Sapphirine-bearing rock, Val Codera, Italy. *American Mineralogist* 49, 146–152.
- 428 Barboza S.A. and Bergantz G.W. (2000) - Metamorphism and anatexis in the mafic complex contact
429 aureole, Ivrea Zone, northern Italy. *Journal of Petrology* 41:1307–1327.
430 <https://doi.org/10.1093/petrology/41.8.1307>
- 431 Beltrando M. , Lister G.S. , Rosenbaum G. , Richards S. and Forster M.A. (2010) - Recognizing
432 episodic lithospheric thinning along a convergent plate margin: The example of the Early Oligocene
433 Alps. *Earth-Science Reviews* 103; 81–98. <https://doi.org/10.1016/j.earscirev.2010.09.001>
- 434 Berger A., Rosenberg C., Schmid S.M. (1996) Ascent, emplacement and exhumation of the Bergell
435 pluton within the Southern Steep Belt of the Central Alps. *Schweizerische Mineralogische und*
436 *Petrographische Mitteilungen* 76:357–382.
- 437 Berger A., Rosenberg C., Schaltegger U. (2009) Stability and isotopic dating of monazite and
438 allanite in partially molten rocks: examples from the Central Alps. *Swiss Journal of Geoscience*
439 102:15–29, <https://doi.org/10.1007/s00015-009-1310-8>
- 440 Bertotti G., Siletto G. B. & Spalla M. I. (1993) Deformation and metamorphism associated with
441 crustal rifting: Permian to Liassic evolution of the Lake Lugano-Lake Como area (Southern Alps).
442 *Tectonophysics*, 226, 271–284. Doi: 10.1016/0040-1951(93)90122-Z
- 443 Brodie K. H., Rex D. & Rutter E. H. (1989) On the age of deep crustal extensional faulting in the
444 Ivrea zone, Northern Italy. Geological Society, London, Special Publications, 45, 203–210.
445 Doi: 10.1144/GSL.SP.1989.045.01.11

- 446 Brouwer F.M., van de Zedde D.M., Wortel M.J. and Vissers R.L. (2004) Late-orogenic heating
447 during exhumation: Alpine PTt trajectories and thermomechanical models. *Earth and Planetary*
448 *Science Letters* 220 (2004) 185-199. [https://doi.org/10.1016/S0012-821X\(04\)00050-0](https://doi.org/10.1016/S0012-821X(04)00050-0)
- 449 Brown M. 2007. Metamorphic conditions in orogenic belts: a record of secular change.
450 *International Geological Review*, 49:193–234, <https://doi.org/10.2747/0020-6814.49.3.193>
- 451 Brown, M., (2008) - Granites, migmatites and residual granulites: relationships and processes. In:
452 Sawyer, E.W., Brown, M. (Eds.), *Working With Migmatites: Mineralogical Association of Canada*
453 *Short Course*, 38, pp. 97–144.
- 454 Burri T., Berger A., Engi M. (2005) Tertiary migmatites in the Central Alps: regional distribution,
455 field relations, conditions of formation, and tectonic implications. *Schweizerische Mineralogische*
456 *und Petrographische Mitteilungen*, 85:215–232
- 457 Clark C., Fitzsimons I.C.W., Healy D., Harley S.L. (2011) - How does the continental
458 crust get really hot? *Elements* 7: 235-240. <https://doi.org/10.2113/gselements.7.4.235>
- 459 Cornelius, H.P. (1916) Ein alpines Vorkommen von Sapphirine. *Cent. Mineral.*, 265-269.
- 460 Cornelius, H.P. & Dittler E. (1929) Zur Kenntnis des Sapphirinvorkommens von Alpe Bresciadega
461 in Val Codera (Italien, Prov. Sondrio). *Neues Jahrbuch Fur Mineralogie-Abhandlungen*, 59, 27-64.
- 462 Cherniak D.J., Watson B.E., Grove M., Harrison T.M. (2004) Pb diffusion in monazite: a combined
463 RBS/SIMS study. *Geochimica et Cosmochimica Acta* 68:829–840.
464 <https://doi.org/10.1016/j.gca.2003.07.012>
- 465 Didier A., Bosse V., Cherneva Z., Gautier P., Georgieva M., Paquette J.L. and Gerdjikov I. (2014).
466 Syn-deformation fluid-assisted growth of monazite during renewed high-grade metamorphism in
467 metapelites of the Central Rhodope (Bulgaria, Greece) *Chemical Geology* 381, 206–222.
468 <https://doi.org/10.1016/j.chemgeo.2014.05.020>
- 469 Davies J.H. & Von Blanckenburg F. (1995) Slab breakoff: A model of lithosphere detachment and
470 its test in the magmatism and deformation of collisional orogens. *Earth and Planetary Science*
471 *Letters*, 129, 85–102. Doi: 10.1016/0012-821X(94)00237-S
- 472 Didier A., Bosse V., Bouloton J., Mostefaoui S., Viala M., Paquette J.L., Devidal J.L., Duhamel R.
473 (2015). NanoSIMS mapping and LA-ICP-MS chemical and U–Th–Pb data in monazite from a
474 xenolith enclosed in ndesite (Central Slovakia Volcanic Field). *Contribution to Mineralogy &*
475 *Petrology* vol.170, p.45, doi:10.1007/s00410-015-1200-1.
- 476 Diella V., Spalla M. I. & Tunesi, A. (1992) Contrasted thermo-mechanical evolutions in the
477 Southalpine metamorphic basement of the Orobic Alps (Central Alps, Italy). *Journal of*
478 *Metamorphic Geology*, 10, 203–219. Doi: 10.1111/j.1525-1314.1992.tb00079.x
- 479 Droop G.T.R. & Bucher-Nurminen K. (1984) Reaction textures and metamorphic evolution of
480 sapphirine-bearing granulites from the Gruf Complex, Italian Central Alps. *Journal of Petrology*, 25,
481 766-803.
- 482 Engi, M., Todd, C.S., Schmatz, D.R., 1995. Tertiary metamorphic conditions in the eastern
483 Lepontine Alps. *Schweizerische Mineralogische und Petrographische Mitteilungen* 75, 347– 369.
- 484 Engi M., Bousquet R. & Berger A. (2004) Explanatory notes to the map: Metamorphic structure of
485 the Alps - Central Alps. *Mitteilungen der Österreichischen Mineralogischen Gesellschaft*, 149, 157-
486 173.
- 487 Galli A., Le Bayon B., Schmidt M.W., Burg J.P., Caddick M.J., Reusser E. (2011) Granulites and
488 charnockites of the Gruf Complex: evidence for Permian ultra-high temperature metamorphism in
489 the Central Alps. *Lithos* 124:17–45. doi:10.1016/j.lithos.2010.08.003
- 490 Galli, A., Le Bayon, B., Schmidt, M.W., Burg, J.P., Reusser, E., Sergeev, S.A., & Larionov, A.
491 (2012). U-Pb zircon dating of the Gruf Complex: disclosing the late Variscan granulitic lower crust

492 of Europe stranded in the Central Alps. *Contributions to Mineralogy and Petrology*, 163(2), 353–
493 378. DOI 10.1007/s00410-011-0676-6

494 Galli A., Le Bayon B., Schmidt M.W., Burg J.P. & Reusser E. (2013) Tectonometamorphic history
495 of the Gruf complex (Central Alps): exhumation of a granulite–migmatite complex with the Bergell
496 pluton. *Swiss Journal of Geoscience*, 106:33–62. DOI 10.1007/s00015-013-0120-1

497 Guevara V.E. & Caddick M.J. (2016) Shooting at a moving target: phase equilibria modelling of
498 high temperature metamorphism. *Journal of metamorphic Geology*, 34, 209–235.
499 doi:10.1111/jmg.12179

500 Harley S.L. (1998). – On the occurrence and characterization of ultrahightemperature crustal
501 metamorphism. *In*: Treloar, P.J., O’Brien, P.J. (Eds.), *What Drives Metamorphism and Metamorphic*
502 *Relations? Geological Society, London, Special Publication*, **138**, p. 81-107.

503 Harley S.L. (2016) – A matter of time: the importance of the duration of UHT metamorphism.
504 *Journal of Mineralogical and Petrological Sciences*, v. 111, p. 50-72. doi:10.2465/jmps.160128

505 Kelly N. M., Harley S. L., & Möller A. (2012). Complexity in the behavior and recrystallization of
506 monazite during high-T metamorphism and fluid infiltration. *Chemical Geology*, 322–323, 192–
507 208. <https://doi.org/10.1016/j.chemgeo.2012.07.00>

508 Kelsey D.E., and Hand M. (2015) - On ultrahigh temperature crustal metamorphism: Phase equilibria,
509 trace element thermometry, bulk composition, heat sources, timescales and tectonic settings.
510 *Geoscience Frontiers* 6, 311 – 356. <http://dx.doi.org/10.1016/j.gsf.2014.09.006>

511 Kelsey D.E., White R.W., Powell R. (2003) – Orthopyroxene-sillimanite-quartz
512 assemblages: distribution, petrology, quantitative P-T-X constraints and P-T paths. *Journal of*
513 *Metamorphic Geology* 21, 439-453. DOI: 10.1046/j.1525-1314.2003.00456.x

514 Köppel V., Günthert A., Grünenfelder M. (1981). Patterns of U–Pb zircon and monazite ages in
515 polymetamorphic units of the Swiss Alps. *Schweizerische Mineralogische und Petrographische*
516 *Mitteilungen* 61, 97–119.

517 Korhonena F.J., Clarka C., Brown M., Bhattacharyac S., Taylora R. (2013) How long-lived is
518 ultrahigh temperature (UHT) metamorphism? Constraints from zircon and monazite geochronology
519 in the Eastern Ghats orogenic belt, India. *Precambrian Research*. Vol. 234, 322-350.
520 doi.org/10.1016/j.precamres.2012.12.001

521 Lardeaux J.M. and Spalla I. (1991) - From granulites to eclogites in the Sesia zone (Italian Western
522 Alps): a record of opening and closure of the Piedmont ocean. *Journal of Metamorphic Geology*,
523 9:35–59

524 Liati A., Gebauer D. (2003) Geochronological constraints for the time of metamorphism in the Gruf
525 Complex (Central Alps) and implications for the Adula-Cima Lunga nappe system. *Schweizerische*
526 *Mineralogische und Petrographische Mitteilungen*, 83:159–172

527 McDade P., Harley S.L. (2001) - A petrogenetic grid for aluminous granulite facies metapelites in
528 the KFMASH system. *Journal of Metamorphic Geology*, p. 19, p. 45 – 59 DOI: 10.1046/j.0263-
529 4929.2000.00296.x

530 Manzotti P., Rubatto D., Darling J., Zucali M., Cenko-Tok B., Engi M. (2012) - From Permo-
531 Triassic lithospheric thinning to Jurassic rifting at the Adriatic margin: Petrological and
532 geochronological record in Valtournenche (Western Italian Alps). *Lithos* 146–147; 276–292.
533 doi:10.1016/j.lithos.2012.05.007

534 Manzotti, P. & Zucali, M. 2013. The pre-Alpine tectonic history of the Austroalpine continental
535 basement in the Valpelline unit (Western Italian Alps). *Geological Magazine*, 150, 153–172. Doi:
536 10.1017/S0016756812000441.

537 Marotta A.M., Roda M., Conte K., Spalla M.I. (2016) Thermo-mechanical numerical model of the
538 transition from continental rifting to oceanic spreading: the case study of the Alpine Tethys.

- 539 Geological Magazine, in press, 1-30. Doi: 10.1017/S0016756816000856.
- 540 Marotta A.M., Gosso G., Spalla M.I. (2009) Upper and lower crustal evolution during lithospheric
541 extension: Numerical modelling and natural footprints from the European Alps. Geological Society
542 Special Publication, 321, 33-72. Doi: 10.1144/SP321.3.
- 543 Montel J.M.(1986) Experimental determination of the solubility of Ce-monazite in SiO₂-Al₂O₃-
544 K₂O-Na₂O melts at 800 °C, 2 kbar, under H₂O-saturated conditions *Geology* v. 14 no. 8 p. 659-662
- 545 Montel J.M., Didier J. & Pichavant M. (1991) Origin of muscovite enclaves in intrusive
546 granites. *Developments in Petrology : Enclaves and Granite Petrology*, 509-528. Elsevier.
- 547 Müntener O., Hermann J. & Trommsdorff V. (2000). Cooling history and exhumation of lower
548 crustal granulite and upper Mantle (Malenco, eastern Central Alps). *Journal of Petrology*, 41, 175–
549 200.
- 550 Niggli E. (1974) Metamorphism and tectonics of the Alps. *Memorie della Società geologica*
551 *Italiana*, 13, 285-289.
- 552 Oalman J., Möller A. & Bousquet R., (2013). P-T modelling reveals juxtaposition of units within
553 the Gruf Complex (Central Alps) during orogenesis. *Mineralogical Magazine*, 77, 1873.
554 DOI:10.1180/minmag.2013.077.5.15
- 555 Oalman J. Möller A. & Bousquet R., (2016) – Unravelling the P-T-t evolution of the crust of the
556 Gruf complex by in situ accessory mineral dating and thermometry combined with P-T modelling
557 of microdomains. European Mineralogical Conference, Rimini.
- 558 Paquette J.L., Goncalves P., Devouard B. and Nicollet C. (2004). Micro-drilling ID-TIMS U-Pb
559 dating of single monazites: A new method to unravel complex poly-metamorphic evolutions.
560 Application to the UHT granulites of Andriamena (North-Central Madagascar). *Contributions to*
561 *Mineralogy and Petrology*, 147: 110–122 DOI: 10.1007/s00410-003-0549-8
- 562 Paquette, J.-L., Tiepolo, M., 2007. High resolution (5 µm) U-Th-Pb isotopes dating of monazite
563 with excimer laser ablation (ELA)-ICPMS. *Chemical Geology* 240, 222–237.
564 DOI:10.1016/j.chemgeo.2007.02.014
- 565 Paquette, J.L., Piro, J.L., Devidal, J.L., Bosse, V., Didier, A., 2014. Sensitivity enhancement in LA-
566 ICP-MS by N₂ addition to carrier gas: application to radiometric dating of U-Th bearing minerals.
567 *Agilent ICP-MS J.* 58, 4–5
- 568 Perchuk A.L., Safonov O.G., Smit C.A., van Reenen D.D., Zakharov V.S, Gerya T.V. (2017)
569 Precambrian ultra-hot orogenic factory: Making and reworking of continental crust;
570 *Tectonophysics*, in press. <https://doi.org/10.1016/j.tecto.2016.11.041>
- 571 Peressini G., Quick J. E., Sinigoi S., Hofmann A. W. & Fanning M. (2007) Duration of a large mafic
572 intrusion and heat transfer in the lower crust: a SHRIMP-U-Pb zircon study in the Ivrea-Verbano
573 Zone (Western Alps, Italy). *Journal of Petrology*, 48, 1185–1218. Doi: 10.1093/petrology/egm014
- 574 Pownall J.M. (2015) - UHT metamorphism on Seram, eastern Indonesia: reaction microstructures
575 and P–T evolution of spinel-bearing garnet–sillimanite granulites from the Kobipoto Complex.
576 *Journal of metamorphic Geology*, 33, 909–935 doi:10.1111/jmg.12153
- 577 Pownall J.M., Hall R., Armstrong R.A. & Forster M.A. (2014) - Earth's youngest known ultrahigh-
578 temperature granulites discovered on Seram, eastern Indonesia. *Geology*, 42, 279–282. DOI:
579 <https://doi.org/10.1130/G35230.1>
- 580 Rapp R.P. & Watson E.B. (1986). Monazite solubility and dissolution kinetics: implications for the
581 thorium and light rare earth chemistry of felsic magmas. *Contributions to Mineralogy and*
582 *Petrology*. 94 : 304-316.
- 583 Redler C., White R.W., Johnson. T.E., (2013) Migmatites in the Ivrea Zone (NW Italy): Constraints
584 on partial melting and melt loss in metasedimentary rocks from Val Strona di Omegna *Lithos* Vol.

585 190–191, March 2014, Pages 1-12. doi.org/10.1016/j.lithos.2013.04.019

586 Rocha B.C., Moraes R., Möller A., Cioffi C.R., Jercinovic M.J. (2017) Timing of anatexis and melt
587 crystallization in the Socorro–Guaxupé Nappe, SE Brazil: Insights from trace element composition
588 of zircon, monazite and garnet coupled to UPb geochronology. *Lithos* 277, 337-355.
589 <https://doi.org/10.1016/j.lithos.2016.05.020>

590 Rubatto D. (2002) Zircon trace element geochemistry: partitioning with garnet and the link between
591 U–Pb ages and metamorphism. *Chemical Geology* 184, 123–138 [doi.org/10.1016/S0009-](https://doi.org/10.1016/S0009-2541(01)00355-2)
592 [2541\(01\)00355-2](https://doi.org/10.1016/S0009-2541(01)00355-2)

593 Rubatto D., Hermann J., Buick I.S., (2006). Temperature and bulk composition control on the
594 growth of monazite and zircon during low-pressure anatexis (Mount Stafford, central Australia).
595 *Journal of Petrology*, 47, 1973–1996. <https://doi.org/10.1093/petrology/egl033>

596 Rubatto D., Hermann J., Berger A., Engi M., (2009). Protracted fluid-present melting during
597 Barrovian metamorphism in the Central Alps. *Contributions to Mineralogy and Petrology*.
598 doi:10.1007/s00410-009-0406-5.

599 Rubatto D., Chakraborty S. and Dasgupta S. (2013) Timescales of crustal melting in the Higher
600 Himalayan Crystallines (Sikkim, Eastern Himalaya) inferred from trace element-constrained
601 monazite and zircon chronology. *Contributions to Mineralogy and Petrology* 165:349–372.
602 doi: [10.1007/s00410-012-0812-y](https://doi.org/10.1007/s00410-012-0812-y)

603 Schaltegger U. (1994) Unravelling the pre-Mesozoic history of Aar and Gotthard massifs (Central
604 Alps) by isotopic dating - a review. *Schweizerische Mineralogische und Petrographische*
605 *Mitteilungen*, 74, 41–51.

606 Schärer U. (1984) The effect of initial ²³⁰Th disequilibrium on young U-Pb ages: the Makalu case,
607 Himalaya. *Earth Planetary Science Letters* 67 : 191-0204.

608 Schmid S.M., Berger A., Davidson C., Gieré R., Hermann J., Nievergelt P., Pusching A.R. &
609 Rosenberg C. (1996) The Bergell Pluton (Southern Switzerland-Northern Italy): overview
610 accompanying a geological-tectonic map of the intrusion and surrounding country rocks.
611 *Schweizerische Mineralogische und Petrographische Mitteilungen*, 76, 329–355.

612 Schmitz S., Möller A., Wilke M., Malzer W., Kannigiesser B., Bousquet R., Berger A., Schefer S.
613 (2009) Chemical U-Th-Pb dating of monazite by 3D-Micro X-ray fluorescence analysis with
614 synchrotron radiation. *European Journal of Mineralogy* 21:927–945. [https://doi.org/10.1127/0935-](https://doi.org/10.1127/0935-1221/2009/0021-1964)
615 [1221/2009/0021-1964](https://doi.org/10.1127/0935-1221/2009/0021-1964)

616 Schuster R., Scharbert S., Abart R. & Frank W. (2001) Permo-Triassic extension and related HT/LP
617 metamorphism in the Austroalpine-Southalpine realm. *Mitteilungen der Gesellschaft der Geologie*
618 *und Bergbaustudenten in Österreich*, 45, 111–141.

619 Schuster R. & Stuewe K. (2008) Permian metamorphic event in the Alps. *Geology*, 36, 603–606.
620 Doi: 10.1130/G24703A.1.

621 Spalla M. I. & Marotta A. M. (2007) P–T evolutions vs. numerical modelling: a key to unravel the
622 Paleozoic to early-Mesozoic tectonic evolution of the Alpine area. *Periodico di Mineralogia*, 76,
623 267–308. Doi: 10.2451/2007PM0029.

624 Spalla M. I., Zanoni D., Marotta A. M., Rebay G., Roda M., Zucali M. & Gosso G. (2014) The
625 transition from Variscan collision to continental break-up in the Alps: insights from the comparison
626 between natural data and numerical model predictions. *Geological Society, London, Special*
627 *Publication*, 405, 363–400. Doi: 10.1144/SP405.11

628 Spear F.S., Pyle J.M. (2002) Apatite, monazite, and xenotime in metamorphic rocks, reviews in
629 mineralogy and geochemistry, phosphates: geochemical, geobiological, and materials importance.
630 *Mineralogical Society of America*, 48:523–558.

631 Stepanov A.S., Hermann J., Rapp R.P., Rubatto D. (2012) Experimental study of monazite/melt

632 partitioning with implications for the REE, Th and U geochemistry of crustal rocks. *Chemical*
633 *Geology*. 300-301:200–220. <https://doi.org/10.1016/j.chemgeo.2012.01.007>

634 Stüwe K. 1995 - Thermal buffering effects at the solidus. Implications for the equilibration of
635 partially melted metamorphic rocks. *Tectonophysics* vol. 248 p. 39-51.

636 Todd, C.S. and Engi, M., 1997. Metamorphic field gradients in the Central Alps. *Journal of*
637 *Metamorphic Geology* 15, 513–530

638 Tribuzio R., Thirlwall M.F., Messiga B. (1999) Petrology, mineral and isotope geochemistry of the
639 Sondalo gabbroic complex (Central Alps, Northern Italy): implications for the origin of post-
640 Variscan magmatism. *Contributions to Mineralogy and Petrology*, 136: 48 – 62.

641 Trommsdorff V., (1966). Progressive Metamorphose kieseliger Karbonatgesteine in den
642 Zentralalpen zwischen Bernina und Simplon. *Schweizerische Mineralogische und Petrographische*
643 *Mitteilungen* 46, 431–460.

644 Vavra G. and Schaltegger, U. (1999) - Post-granulite facies monazite growth and rejuvenation
645 during Permian to Lower Jurassic thermal and fluid events in the Ivrea Zone (Southern Alps).
646 *Contributions to Mineralogy and Petrology*, 134: 405 – 414

647 Vielzeuf, D. and Holloway, J.R. (1988). Experimental determination of the fluid-absent melting
648 reactions of pelitic rocks — consequences for the crustal differentiation. *Contributions to*
649 *Mineralogy and Petrology*, 98, 257–276.

650 Von Blanckenburg F. & Davies J.H. (1995) Slab breakoff. A model for syncollisional magmatism
651 and tectonics in the Alps. *Tectonics*, 14, 120–131. Doi: 10.1029/94TC02051

652 Wenk H.R., Wenk E. and Wallace J.H. (1974) Metamorphic mineral assemblages in pelitic rocks of
653 the Bergell Alps. *Schweizerische Mineralogische und Petrographische Mitteilungen*, 54:507-554

654 Whitney D.L. & Evans B.W., 2010. Abbreviations for names of rock-forming minerals. *American*
655 *Mineralogist*, 95, 185–187. DOI: 10.2138/am.2010.3371

656

657 **Figures captions**

658 **Fig.1:** Sketch map of the Gruf complex in the eastern Central Alps after Galli et al., (2011);
659 Asterisk locates upper Val Codera. The sketch is located in the Alpine chain (inset).

660 **Fig. 2:** Microphotographs of the parageneses and textures of the granulitic rock (Plane-
661 (PPL) and cross (XPL)-polarized light; **(a):** The Spr bearing granulitic paragenesis (PPL); **(b):**
662 Complex retrograde symplectites in the Spr bearing portion of the rock granulite with spr2, sp, cord,
663 sil2. Opx + Crd symplectites replace Grt (PPL); **(c):** Spr2+crd resulting of the retrograde reaction
664 Opx + Sil = Spr + Crd (PPL); **(d):** the charnockitic paragenesis (XPL); **(e):** textures of incipient
665 melting or residual melt after extraction in the charnockite portion of the rock (XPL). Abbreviations
666 in text and figures are from Whitney and Evans (2010).

667 **Fig. 3:** Al₂O₃ profiles in the primary Opx (C: core and R: rim) and Al₂O₃ concentrations
668 (contents values) in the Opx from the Opx + Crd symplectite (sym) around garnet.

669 **Fig. 4 (a):** Resorbed crystals of zircons included in primary phenocrysts, Spr and Sil (PPL);

670 (b): Cathodoluminescence images of zircons in the Crd – Bt matrix with oscillatory zoning; (c):
671 zircon grains surrounded by highly luminescent rim (<5 µm to 15 µm) with euhedral faces with
672 Alpine or intermediate ages ($^{206}\text{Pb}/^{238}\text{U}$ ages; 2σ)

673 **Fig. 5 (a):** Monazite inclusions in the phenocrysts (PPL) of Sapphirine and Al-rich
674 orthopyroxene of the Spr bearing domain of the rock; (b): Monazite inclusions in an Opx of the
675 charnockite portion of the rock; note the tiny overgrowths (rich in Y) in the BSE image (crystal
676 T14M1). Circles: $^{208}\text{Pb}/^{232}\text{Th}$ ages in Ma (with ± 1.1 Ma for all data).

677 **Fig. 6 (a):** BSE images of figure 2b and of the monazites in Spr, Crd and in clusters in late
678 symplectites; cathodoluminescence of a zircon in Crd. ThO_2 and Y_2O_3 X-ray maps (spots; in wt%)
679 in the crystal T50M1 and $^{208}\text{Pb}/^{232}\text{Th}$ ages (circles) ages in Ma (with ± 1.1 Ma for the monazites).
680 Black inclusions are needles of sillimanite; arrows: diamond-shaped basal sections.

681 **Fig. 6 (b):** ThO_2 and Y_2O_3 X-ray maps (spots; in wt%) and BSE image and $^{208}\text{Pb}/^{232}\text{Th}$ ages
682 (circles) ages in Ma with $\pm 1.1\text{Ma}$ for a monazite in the charnockite portion of the rock (crystal
683 T12M1).

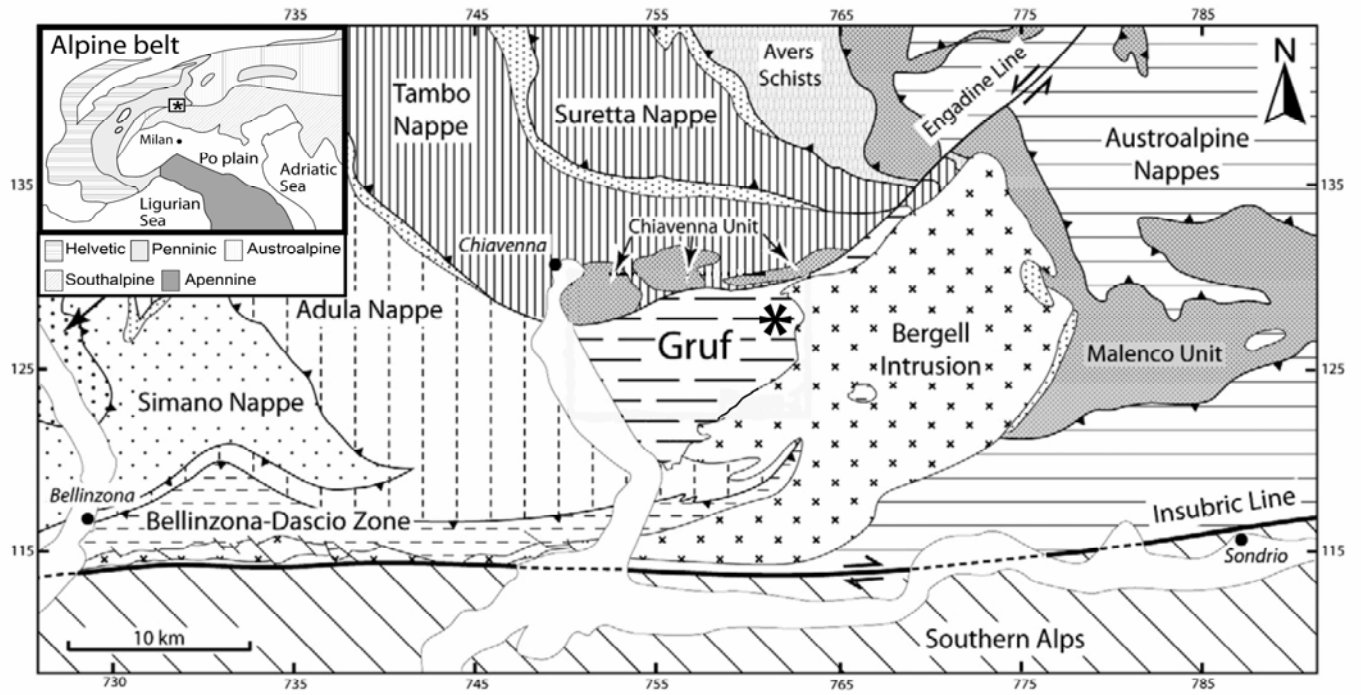
684 **Fig. 7:** Chemical composition of the monazites; (a): Ternary diagram showing the relative
685 Y_2O_3 , ThO_2 and UO_2 (wt%) contents; (b): Y_2O_3 versus Gd_2O_3 ; (c): La_2O_3 versus Gd_2O_3 .

686 **Fig. 8:** Geochronological results; (a): $^{208}\text{Pb}/^{232}\text{Th}$ versus $^{206}\text{Pb}/^{238}\text{U}$ diagram for the
687 monazite; (b): Weighted average $^{208}\text{Pb}/^{232}\text{Th}$ ages in monazite; (c): Tera Wasserburg diagram
688 showing the zircon and monazite data (for more clarity, only concordant U/Pb data are shown); (d):
689 Tera Wasserburg diagram showing U/Pb results for zircon cores with U content ≤ 1000 ppm and
690 zircon grain without apparent Alpine rim in CLI.

691 **Table 1:** Electron microprobe analyses of the monazites. G = granulite domain; Ch =
692 charnockite domain.

Table 1 : analyses of monazites.

Analyses	G			G			G			Ch			G		Ch		G		G	G	G	G
	2	7	14	17	18	23	25	32	33	34	42	45	49	53	56	57	58	59	61	64		
	T50 - M2	T50-M1		i saphirine	T50 - cluster			T14 M1			T13 M1		T12-M1		T10bis-M2		T10 bis	T10bisM1	T18-i OPX	T33-i OPX		
SiO2	0.17	0.27	0.12	0.19	0.21	0.10	0.16	0.25	0.31	0.47	0.22	0.38	0.39	0.59	0.41	0.32	0.19	1.34	0.19	0.32		
P2O5	30.15	29.51	29.77	29.54	29.93	29.99	29.67	30.20	29.96	29.65	30.29	29.57	30.02	29.09	29.60	29.57	29.80	27.70	29.65	30.12		
Ce2O3	29.92	28.92	30.59	29.74	29.23	30.28	29.79	25.18	25.44	25.61	28.36	25.20	24.73	25.71	29.57	29.48	29.22	30.89	29.94	27.14		
La2O3	13.58	13.48	14.31	13.26	13.14	13.30	13.59	10.70	11.09	11.10	12.51	11.39	10.70	11.22	13.47	13.39	13.20	14.78	13.59	12.29		
Pr2O3	3.30	3.18	3.10	3.39	3.19	3.45	3.21	2.78	2.98	2.87	2.93	3.01	2.77	2.89	3.08	3.09	3.23	3.65	3.05	3.02		
Nd2O3	11.49	10.97	11.95	11.58	11.36	11.32	11.06	9.88	10.44	10.49	10.75	8.71	10.32	11.27	11.65	11.66	10.92	11.99	10.52	11.02		
Sm2O3	1.95	1.46	1.54	1.66	1.74	2.17	1.66	2.14	1.90	2.03	1.92	1.64	1.85	1.82	1.73	1.52	1.75	1.19	1.77	1.74		
Gd2O3	1.33	0.44	0.69	1.09	1.54	1.58	1.06	2.44	1.91	2.05	1.39	1.01	2.04	1.60	1.07	1.11	1.01	0.64	0.91	1.82		
Y2O3	0.39	0.13	0.35	0.31	0.50	0.69	0.32	4.78	3.78	3.24	0.98	0.47	3.89	2.63	0.27	0.58	0.91	0.14	0.65	2.14		
CaO	1.34	1.75	1.16	1.39	1.45	1.15	1.46	1.61	1.76	1.77	1.83	2.90	1.78	1.67	1.31	1.45	1.53	0.44	1.53	1.49		
ThO2	5.79	8.43	5.15	6.42	6.07	3.92	6.73	7.84	8.75	9.32	6.78	10.82	9.59	10.07	7.17	5.74	5.19	6.96	5.48	8.00		
UO2	0.98	0.33	0.50	0.78	0.83	1.35	0.75	0.74	0.41	0.32	2.05	3.50	0.40	0.26	0.45	1.29	2.01	0.20	1.78	0.37		
PbO	0.03	0.00	0.00	0.04	0.01	0.00	0.00	0.00	0.03	0.00	0.01	0.02	0.00	0.01	0.00	0.00	0.01	0.00	0.03	0.01		
Total	100.41	98.87	99.23	99.38	99.20	99.30	99.48	98.54	98.76	98.93	100.00	98.63	98.49	98.83	99.76	99.21	98.96	99.90	99.08	99.47		
Si	0.007	0.011	0.005	0.007	0.008	0.004	0.007	0.010	0.012	0.018	0.009	0.015	0.015	0.023	0.016	0.013	0.007	0.054	0.008	0.012		
P	0.996	0.991	0.995	0.990	0.997	0.999	0.992	0.995	0.991	0.984	0.998	0.990	0.993	0.975	0.987	0.988	0.995	0.941	0.992	0.995		
Ce	0.427	0.420	0.442	0.431	0.421	0.436	0.431	0.359	0.364	0.368	0.404	0.365	0.354	0.373	0.426	0.426	0.422	0.454	0.433	0.388		
La	0.195	0.197	0.208	0.194	0.191	0.193	0.198	0.154	0.160	0.161	0.179	0.166	0.154	0.164	0.196	0.195	0.192	0.219	0.198	0.177		
Pr	0.047	0.046	0.045	0.049	0.046	0.049	0.046	0.039	0.042	0.041	0.042	0.043	0.039	0.042	0.044	0.044	0.046	0.053	0.044	0.043		
Nd	0.160	0.155	0.169	0.164	0.160	0.159	0.156	0.137	0.146	0.147	0.149	0.123	0.144	0.159	0.164	0.164	0.154	0.172	0.149	0.153		
Sm	0.026	0.020	0.021	0.023	0.024	0.029	0.023	0.029	0.026	0.027	0.026	0.022	0.025	0.025	0.023	0.021	0.024	0.016	0.024	0.023		
Eu	0.000	0.000	0.000	0.000	0.000	0.000	0.000	0.000	0.000	0.000	0.000	0.000	0.000	0.000	0.000	0.000	0.000	0.000	0.000	0.000		
Gd	0.017	0.006	0.009	0.014	0.020	0.021	0.014	0.031	0.025	0.027	0.018	0.013	0.026	0.021	0.014	0.015	0.013	0.009	0.012	0.023		
Y	0.008	0.003	0.007	0.006	0.010	0.015	0.007	0.099	0.079	0.068	0.020	0.010	0.081	0.055	0.006	0.012	0.019	0.003	0.014	0.044		
Ca	0.056	0.074	0.049	0.059	0.061	0.048	0.062	0.067	0.074	0.075	0.076	0.123	0.074	0.071	0.055	0.062	0.064	0.019	0.065	0.062		
Th	0.051	0.076	0.046	0.058	0.054	0.035	0.060	0.069	0.078	0.083	0.060	0.097	0.085	0.091	0.064	0.052	0.047	0.064	0.049	0.071		
U	0.008	0.003	0.004	0.007	0.007	0.012	0.007	0.006	0.004	0.003	0.018	0.031	0.004	0.002	0.004	0.011	0.018	0.002	0.016	0.003		
Pb	0.000	0.000	0.000	0.000	0.000	0.000	0.000	0.000	0.000	0.000	0.000	0.000	0.000	0.000	0.000	0.000	0.000	0.000	0.000	0.000		
Summe	2.000	2.001	2.001	2.002	1.999	2.000	2.001	1.997	1.999	2.001	1.998	2.000	1.995	2.001	1.999	2.003	2.001	2.006	2.003	1.995		

**Figure 1**

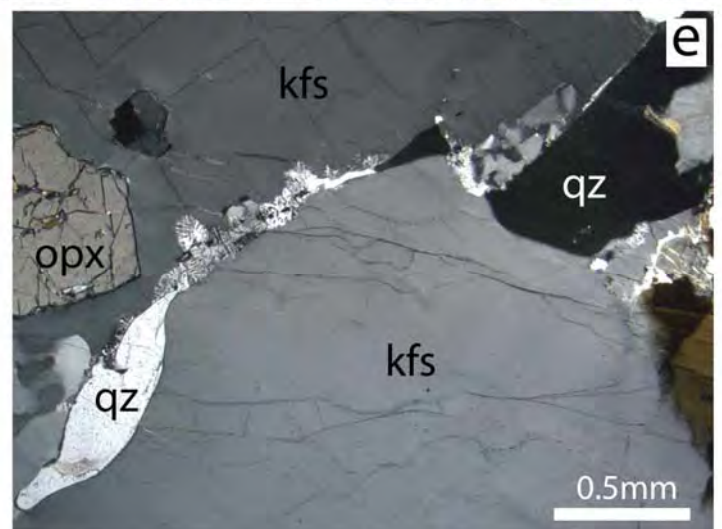
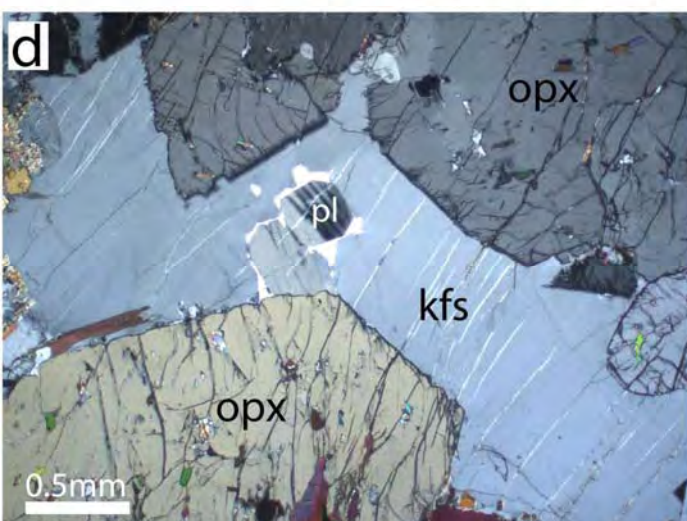
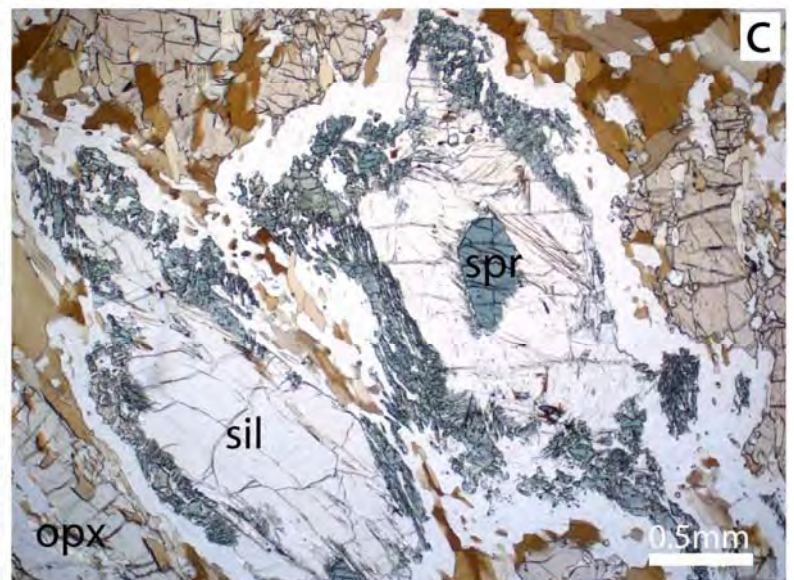
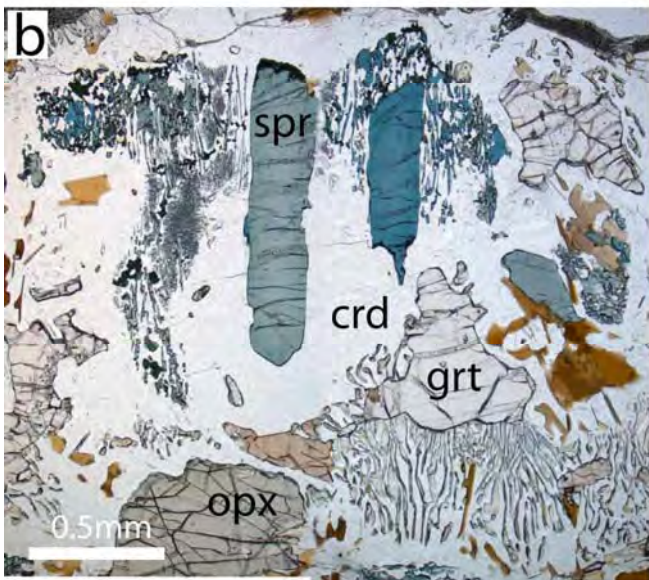
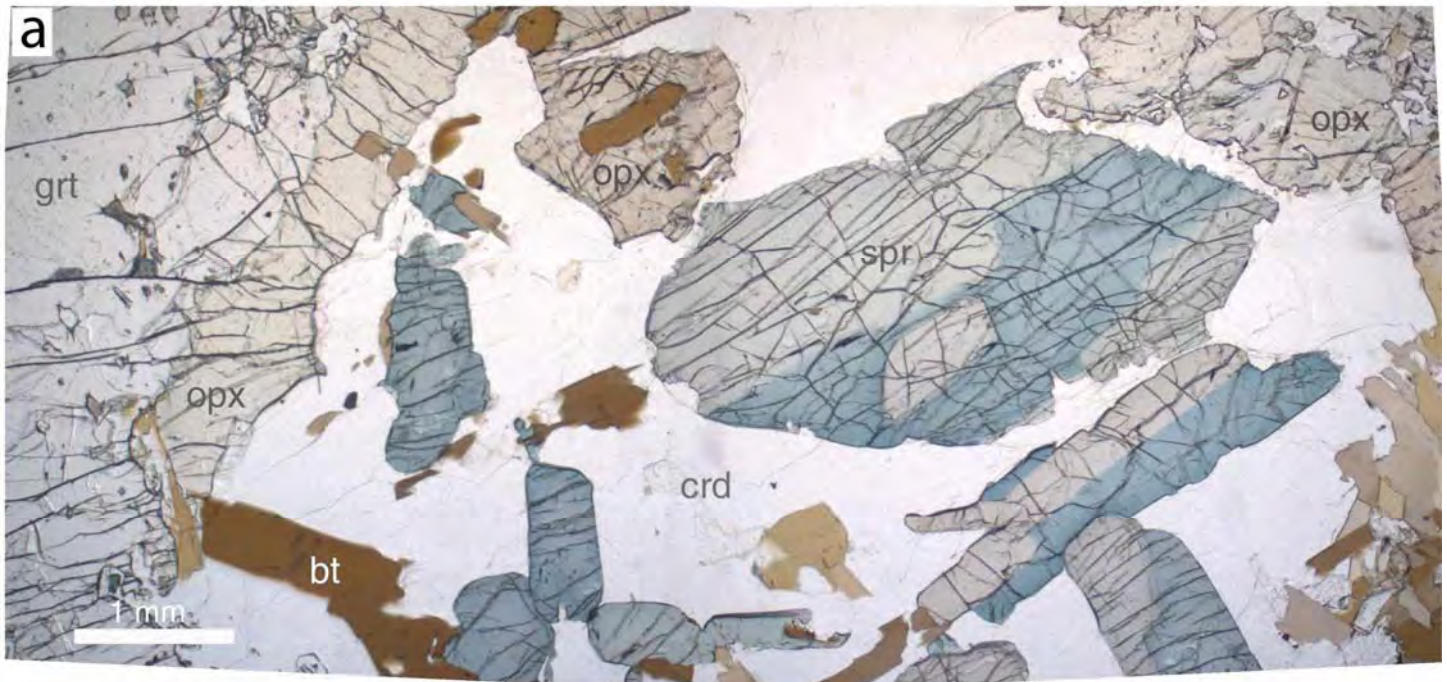


Figure 2

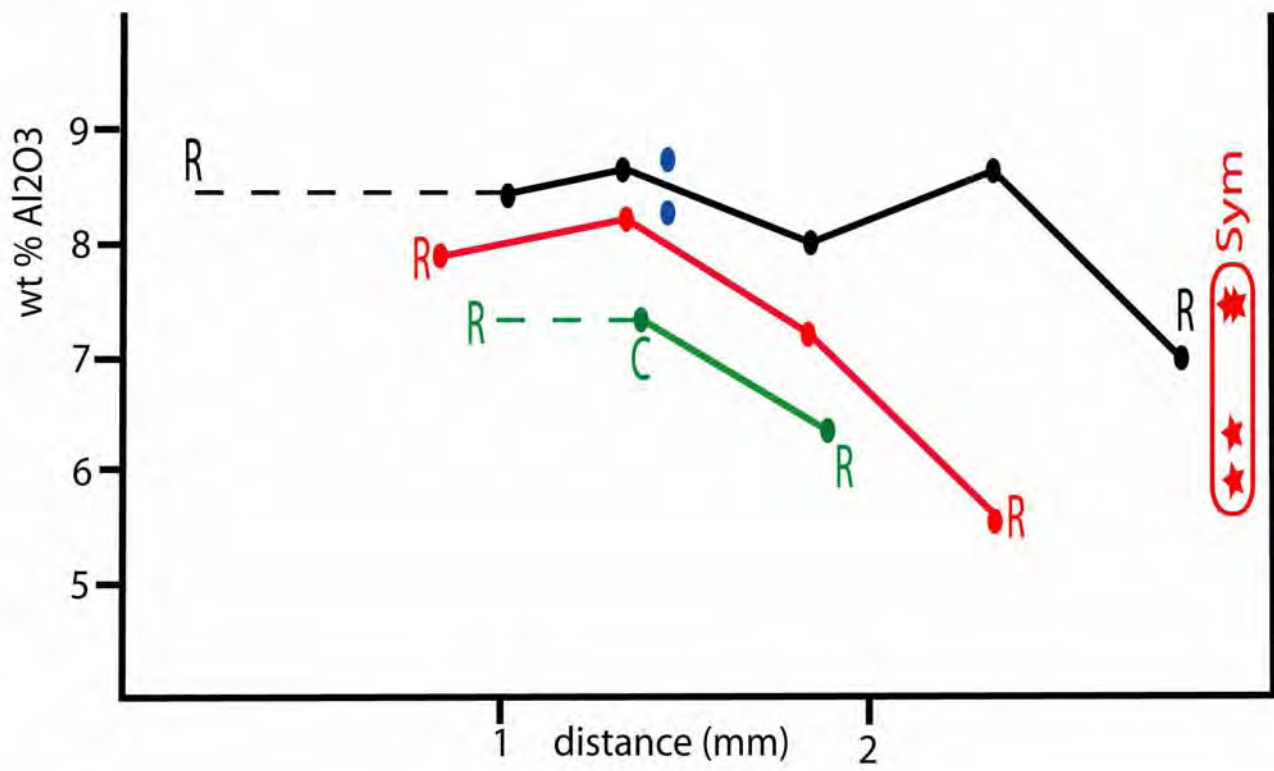


Figure 3

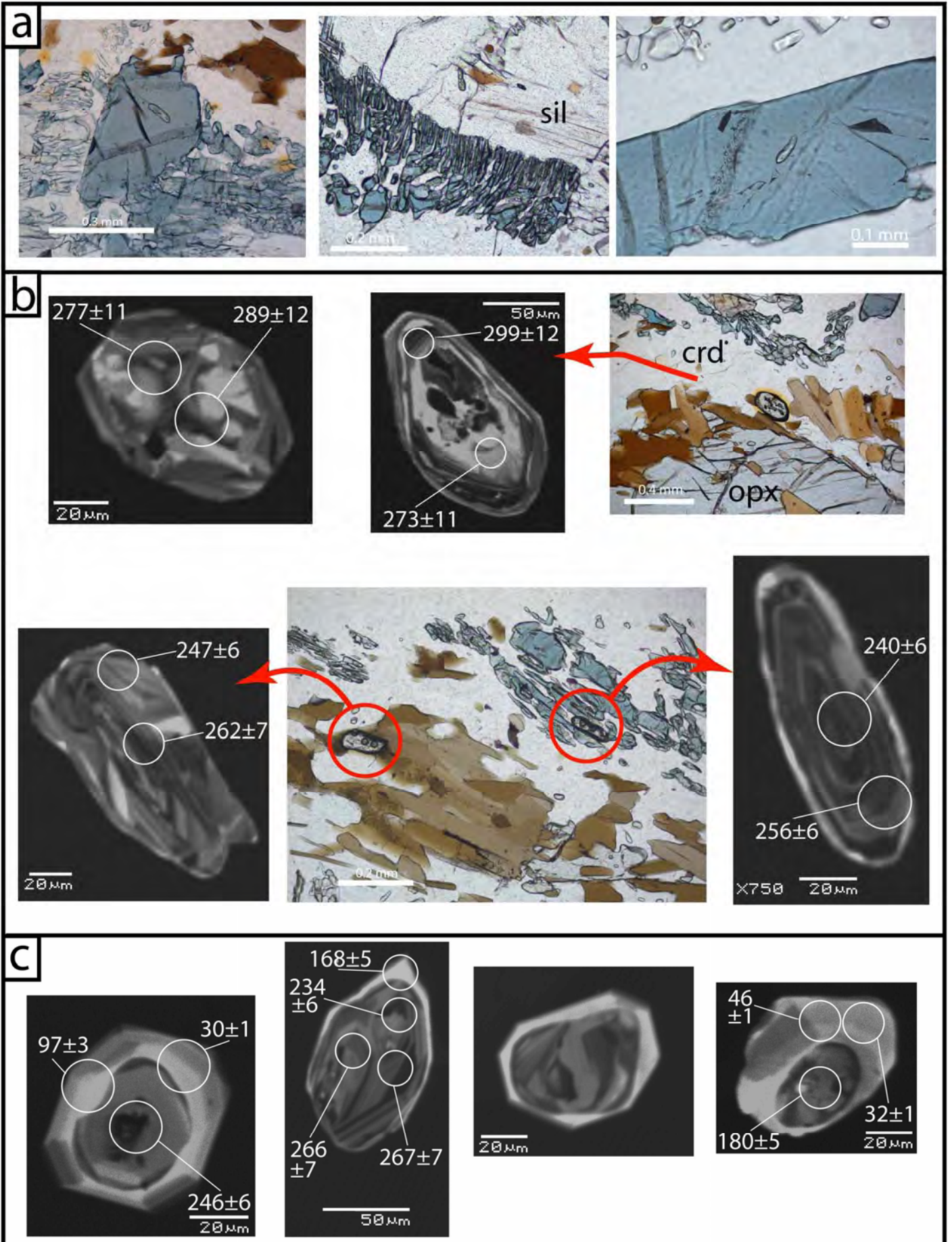


Figure 4

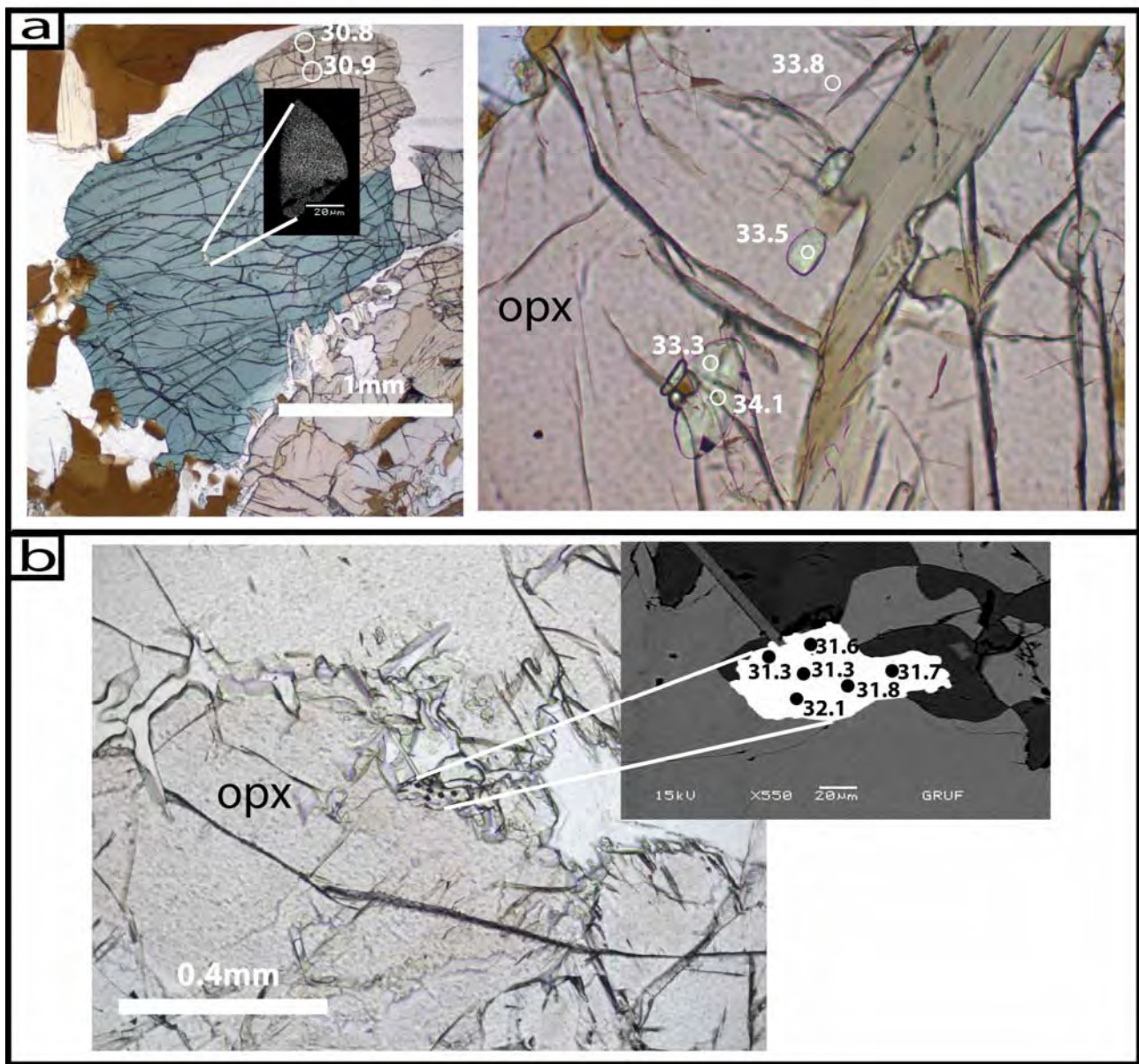


Figure 5

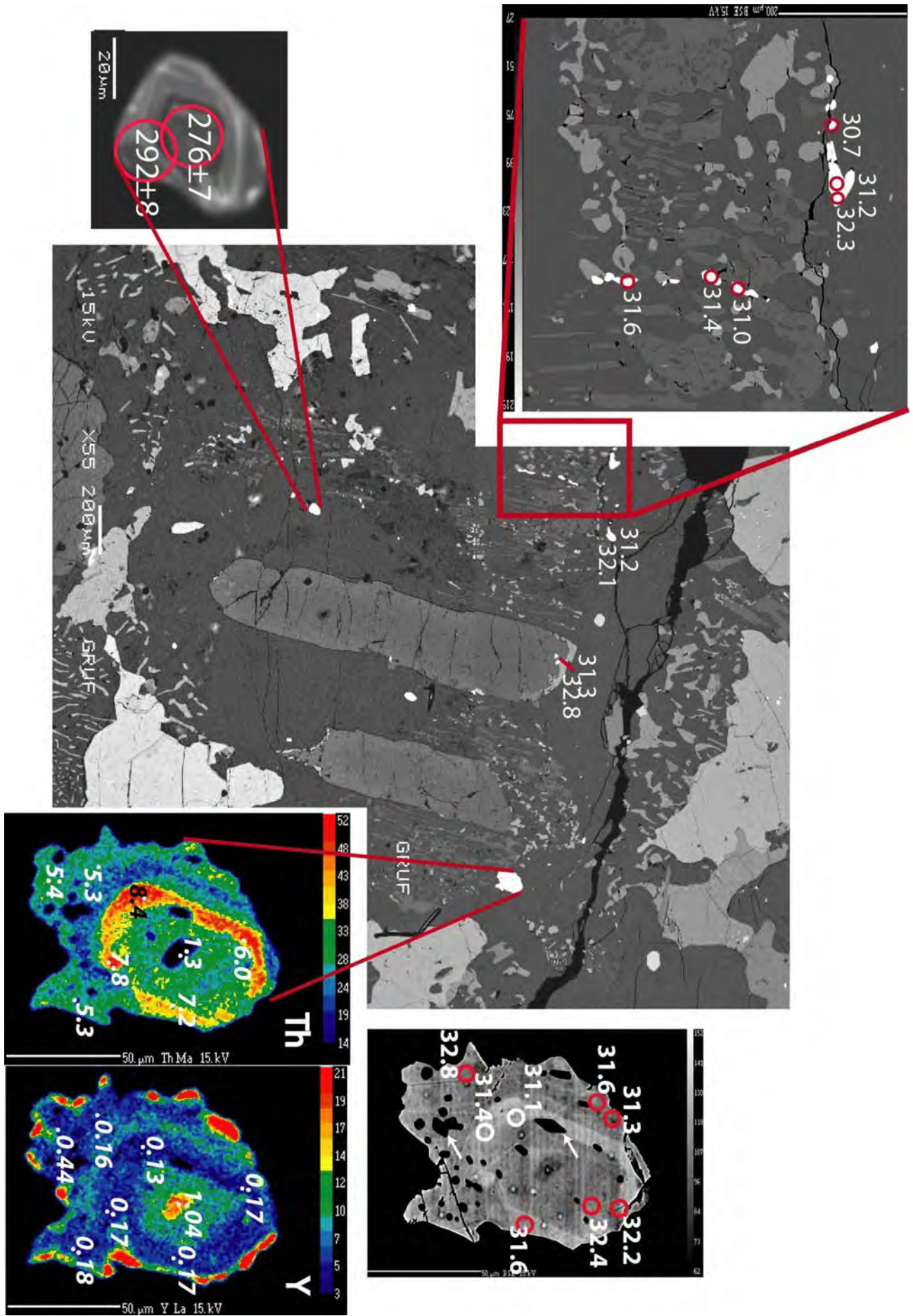


Figure 6a

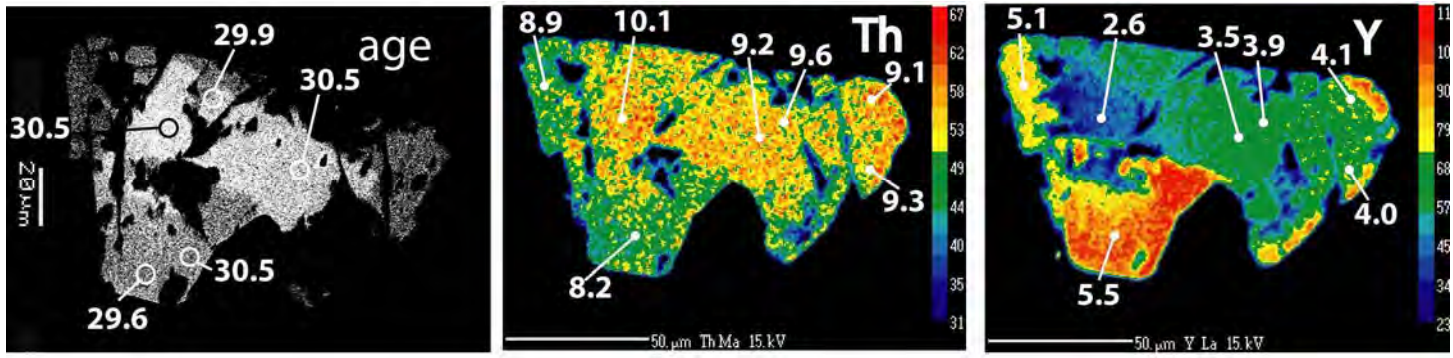


Figure 6b

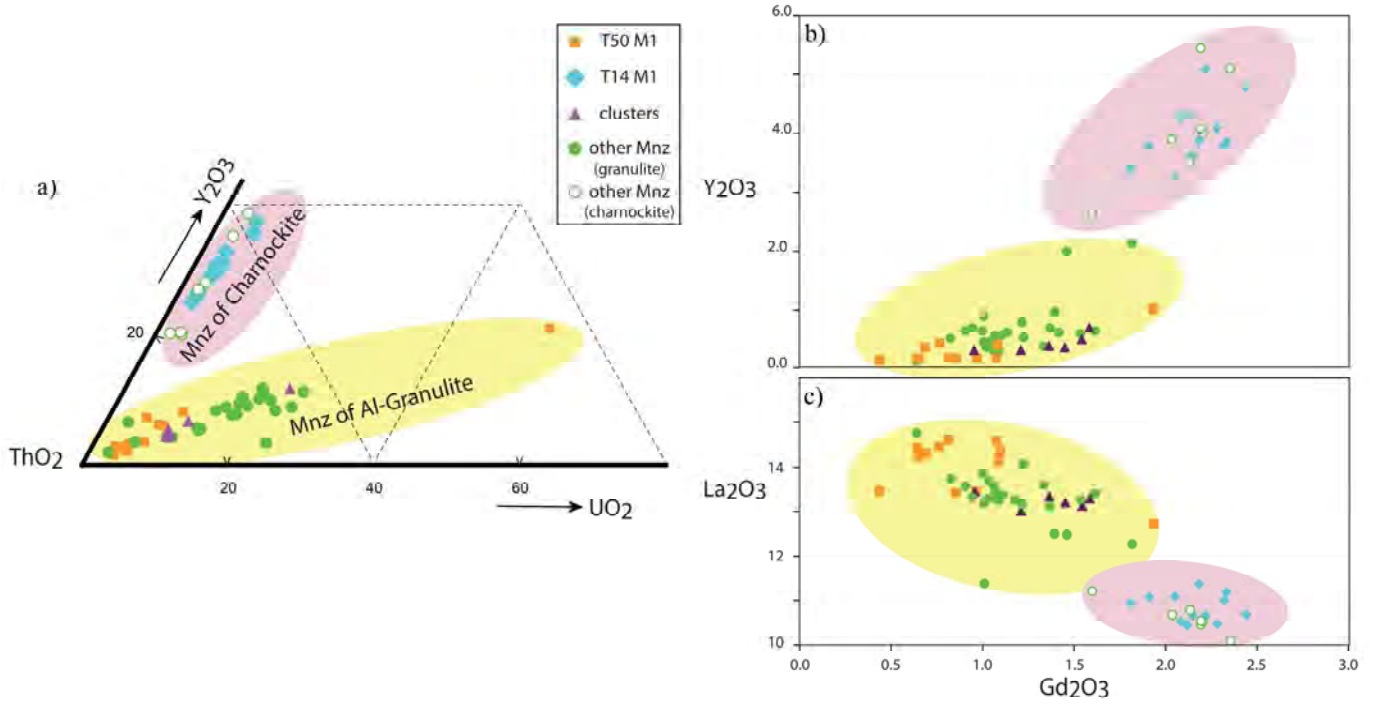


Figure 7

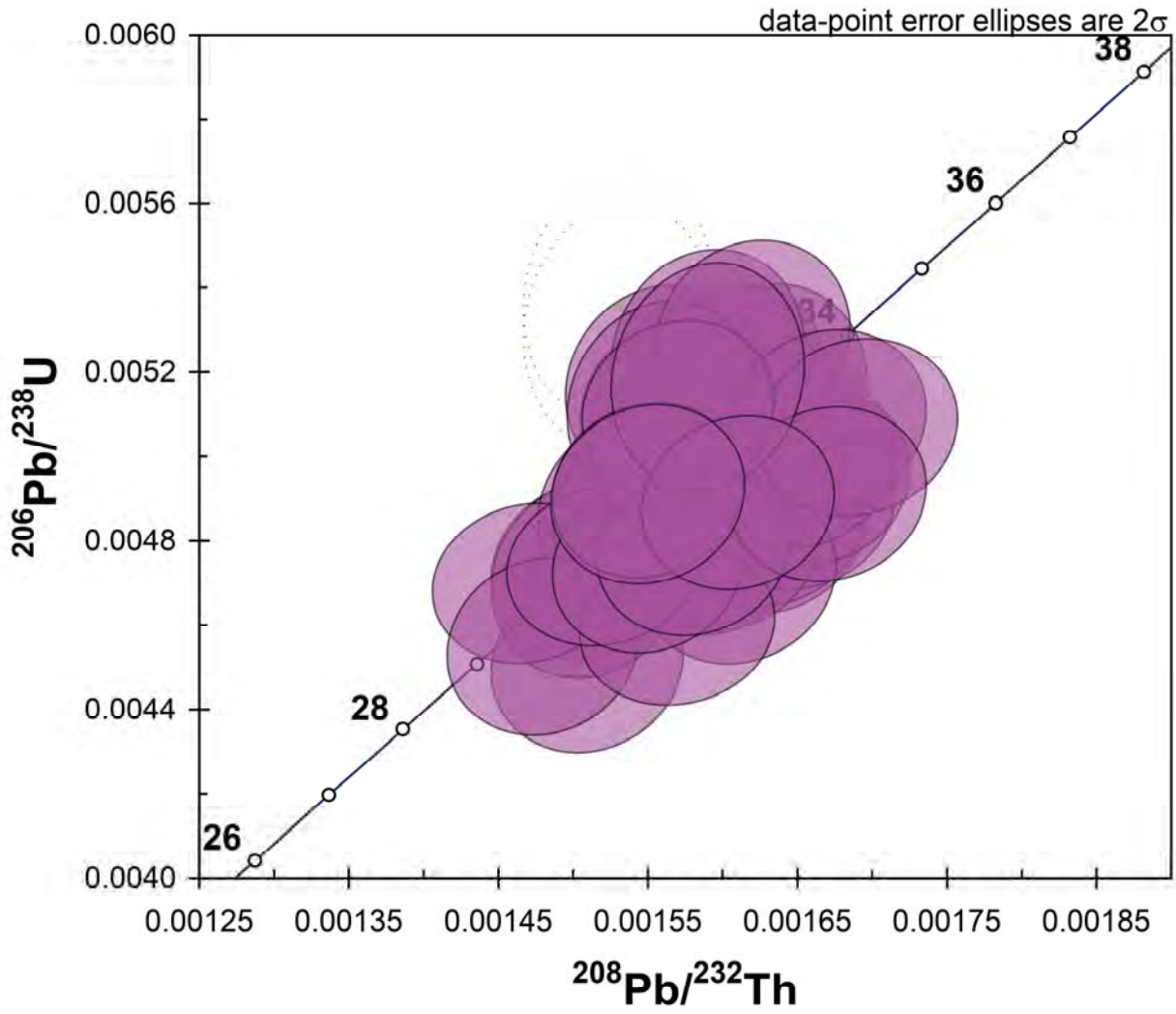


Figure 8 a

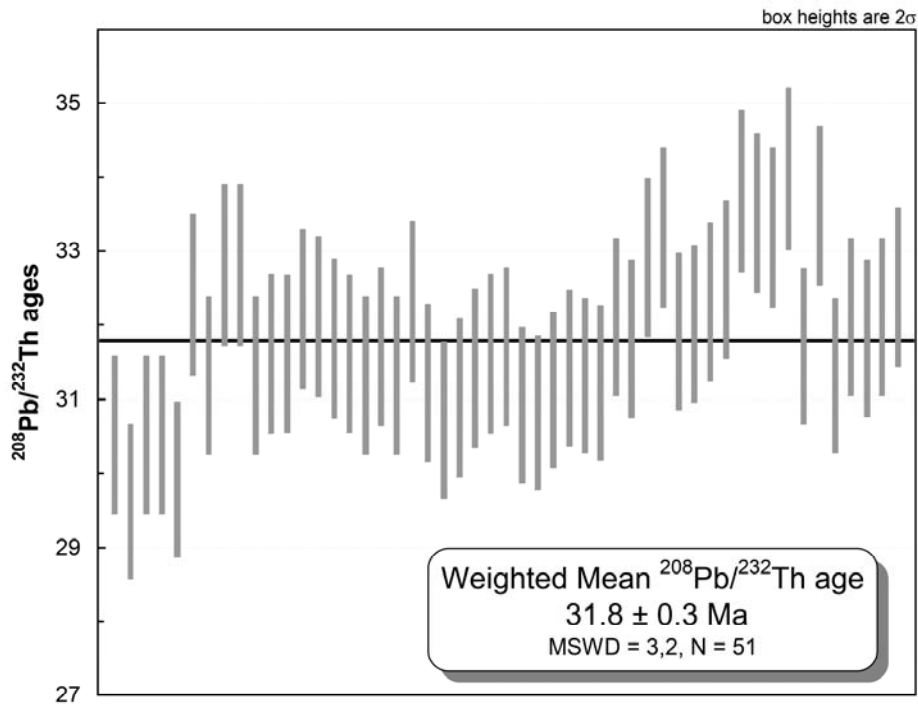


Figure 8 b

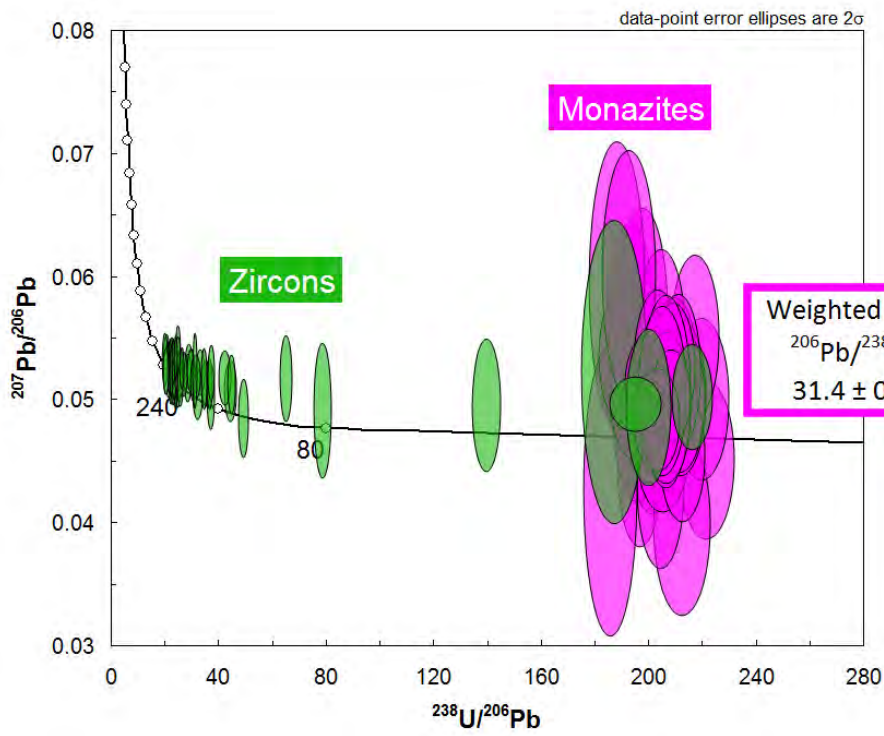


Figure 8c

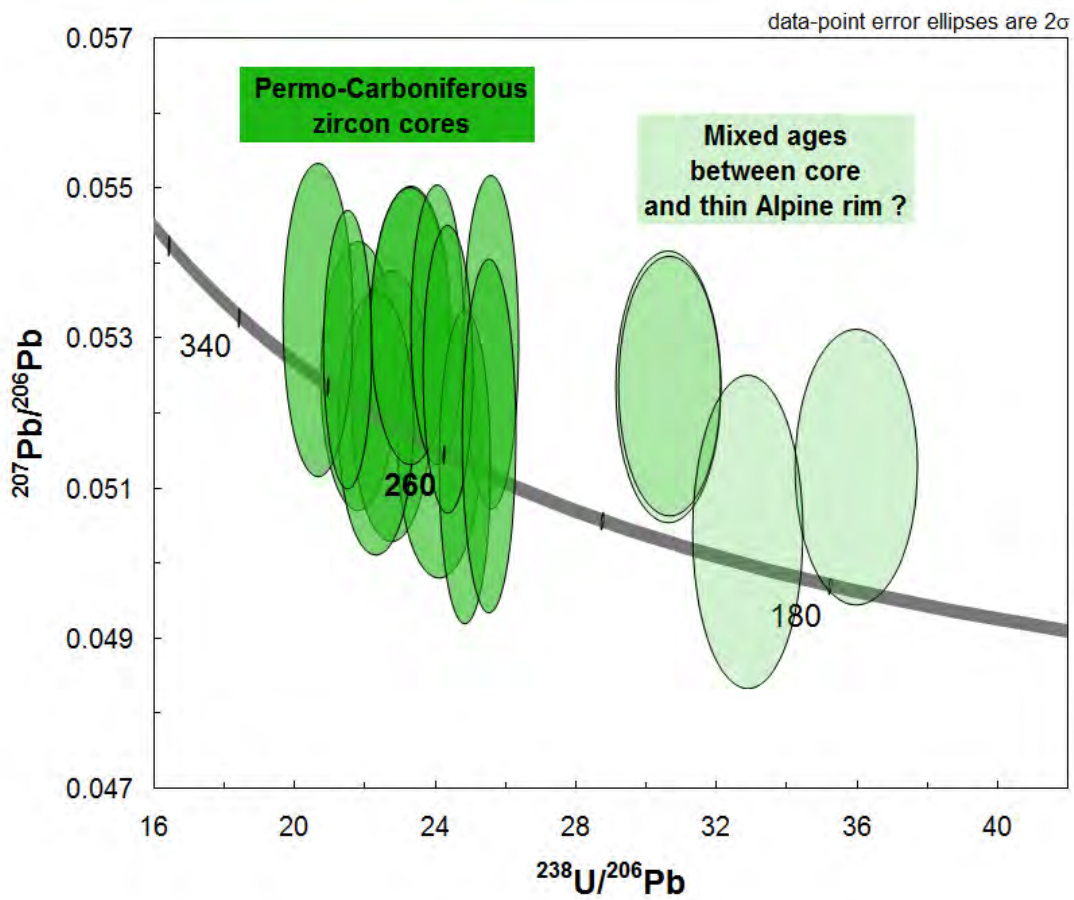


Figure 8 d